TÉCNICO LISBOA

Nanoreactors for Continuous Flow Processing: Effect of Catalyst Loading and Space-Time

Andreia Johns Lopes

Thesis to obtain the Master of Science Degree in

Chemical Engineering

Supervisors:
Prof. Pedro Teixeira Gomes (IST)
Prof. Jan van Hest (TU/e)

Examination Committee:
Chairperson: Professor Carlos Manuel Faria de Barros Henriques (IST)
Supervisor: Professor Pedro Manuel Machado Teixeira Gomes (IST)
Member of the Comittee: Professor Carla Isabel Costa Pinheiro (IST)

November 2018

*“**What lies behind us and what lies before us***
are tiny matters compared to
***what lies within us**."*
-Ralpho Waldo Emerson

Acknowledgements

Initially, I would like to thank Prof. Pedro T. Gomes, my IST supervisor, for introducing to me the Erasmus + Traineeship program, and helping me with the application process to do an internship at the Eindhoven University of Technology, an experience which highly contributed to my professional and personal growth, as it allowed me to develop my skills and helped me gain a sense of independence. I also appreciate his patience and guidance through the writing process of my dissertation.

I would also like to thank my supervisor from TU/e, M. Teresa de Martino for always motivating and supporting me throughout this research and for the time that she spent to explain to me all that I needed to know. I am also grateful to Prof. Jan van Hest for giving me the opportunity to be a part of his research group at TU/e and everybody in the Bio-Organic Chemistry research group who helped me to learn new techniques that enabled me to move forward in this study.

I am thankful to all my friends that have supported me during these five years at IST, and to my friends and colleagues at TU/e that made my time in the Netherlands a great experience. I am also glad that I had friendly housemates during my stay abroad that made the experience even more fun.

Finally, my sincere gratitude goes to my family for all their prayers and for always encouraging me, especially to my parents without your unconditional love and support, this would not have been possible. There are not enough words to express how grateful I am to them, but I hope to take all the morals and values they have inculcated in me and build a life with them as my foundation.

Abstract

Nanoreactors are fascinating structures that sparked the attention of researchers due to their handling of chemical transformations[1]. Employing a nanosized reactor has become an emerging trend since they have the ability of accommodating compounds that will act *in situ*[2][3]. Polymeric nanoreactors (polymersomes) are relevant for catalytic processes due to their robustness, which facilitates recycling and efficient usage of catalytic species[4][5]. Polymersomes can acquire a bowl-shape (stomatocytes) under mild conditions[6] thanks to their flexible membrane allowing a more effective entrapment of catalysts inside the “stomach”. Since management of resources is a guideline for scientists[7], nanoreactors can be beneficial by minimizing reaction waste[8] and cost, as opposed to traditional catalytic pathways. In light of the green chemistry concept[9], the focus was on developing novel catalytic nanoreactors to improve the efficiency of synthetic operations that can be employed for in flow synthesis of compounds, specifically in the hydrolysis of p-nitrophenyl acetate to p-nitrophenol catalyzed by the enzyme *Candida Antarctica Lipase B* (Cal B). The biocatalytic nanosystems engineered, based on polymersomes made using PEG_{44}-PS_{140} copolymers produced by ATRP, were well defined in terms of morphology and shape. Their performance in a continuous flow setup was studied in terms of activity and leaching together with the reusability and a way of optimizing the system in smaller volumes has been reported.

Key-words: *nanoreactors, stomatocytes, continuous flow, reusability, leaching, optimization*

Resumo

Nanoreatores são estruturas fascinantes que despertaram o interesse de cientistas devido à sua maneira de lidar com transformações químicas. A utilização de nanoreactores representa uma tendência emergente, uma vez que têm a capacidade de acomodar compostos que actuam *in situ*. Os nanoreatores poliméricos ("polymersomes") são relevantes para processos catalíticos dado a sua robustez que facilita a reciclagem e o uso eficiente das espécies catalíticas. Sob condições suaves, os nanoreatores poliméricos podem adquirir a forma de "tigela" ("stomatocytes") graças à flexibilidade da sua membrana, oferecendo uma capacidade de encapsulação superior no espaço interior da sua cavidade. Sendo fundamental a gestão de recursos, os nanoreactores podem ser benéficos na minimização de resíduos químicos e dos custos envolvidos, em comparação com processos catalíticos convencionais. À luz do conceito de "química verde", pretendeu-se desenvolver nanoreatores poliméricos inovadores para melhorar a eficiência de operações sintéticas e que possam ser usados em processos de produção contínua, particularmente na hidrólise de p-nitrofenil acetato a p-nitrofenol catalizada pela enzima *Candida Antarctica Lipase B* (Cal B). Os nanosistemas biocatalíticos desenvolvidos, baseados em nanoreatores poliméricos feitos a partir de copolímeros PEG_{44}-PS_{140} produzidos por ATRP, foram bem definidos em termos de morfologia e forma. O seu desempenho num sistema de produção contínua foi estudado em relação à sua estabilidade, tendo-se descrito também a sua capacidade de reutilização e uma forma de optimizar o sistema em pequenos volumes reaccionais.

Palavras-chave: nanoreatores, *stomatocytes*, produção contínua, reutilização, estabilidade, optimização

Table of Contents

List of Figures

List of Tables

List of Abbreviations

AF4	Asymmetric Flow Field-Flow Fractionation
ATRP	Atom Transfer Radical Polymerization
BSA	Bovine serum albumin
Cal B	Candida Antarctica Lipase B
cryo-TEM	Cryo- Transmission Electron Microscopy
DLS	Dynamic Light Scattering
DMSO	Dimethylsulfoxide
DTT	Dithiothreitol
EDTA	Ethylenediaminetetraacetic acid
EM	Electron Microscopy
HPLC	High Performance Liquid Chromatography
ID	Internal diameter
PAA	Poly(acrylic acid)
PAA-*b*-PS	Poly(acrylic acid)-*block*-polystyrene
PCS	Photon Correlation Spectroscopy
PdI	Polydispersity index
PDMS	Poly(dimethylsiloxane)
PEG	Poly(ethylene glycol)
PEG-*b*-PS	Poly(ethylene glycol)-*b*-polystyrene
PHPMA	Poly(*N*-hydroxypropyl)methacrylamide
PMDETA	*N*,*N*,*N*′,*N*″,*N*‴-Pentamethyldiethylenetriamine
PMOXA	Poly(methyloxazolidine)
PNIPAM-*b*-PEO	Poly(*N*-isopropylacrylamide)-*b*-poly(ethylene oxide
p-NP	*para*-Nitrophenol
p-NPA	*para*-Nitrophenyl acetate
PS	Polystyrene
PS-*b*-PIAT	Polystyrene-*b*-polyisocyanopeptide
QUELS	Quasi Elastic Light Scattering
RAFT	Reversible Addition Fragmentation Chain-Transfer
SDS-PAGE	Sodium dodecyl sulfate-polyacrylamide gel electrophoresis
SEC	Size Exclusion Chromatography
SEM	Scanning Electron Microscopy
TEM	Transmission Electron Microscopy
THF	Tetrahydrofuran
ODEs	Ordinary differential equations
MW	Molecular weight

List of Symbols

[E]	enzyme concentration
[S]	substrate concentration
[ES]	enzyme-substrate concentration
$[E_T]$	total enzyme concentration
[P]	product concentration
k_{on}	binding of substrate to enzyme rate constant
k_{off}	dissociation of the enzyme-substrate complex rate constant
k_{cat}	transition from substrate to product rate constant (with the aid of the enzyme)
v	enzymatic rate
V_{max}	maximum rate
K_M	Michaelis-Menten constant
Re	Reynolds number
ρ	fluid density
u	flow velocity
D	characteristic length
μ	dynamic viscosity
Pe	Peclet number
L	effective length
D	dispersion coefficient (Pe)/translational diffusion coefficient (d_H)
Bo	Bodenstein number
D_{ax}	axial dispersion
Da_M	Damkőhler number
τ_t	transport time
τ_r	reaction time
d_H	hydrodynamic diameter
k	Boltzmann's constant
T	absolute temperature/ transmittance
η	viscosity
G(τ)	correlation function
I	intensity
t	time
τ	delay time for G(τ)
τ	space-time (to calculate the productivity of p-NP)
n	refractive index of dispersant
λ_0	wavelength of laser
θ	scattering angle
I_t	intensity of transmitted light
I_0	intensity of incident light
A	absorbance

ε	molar absorptivity
l	path length
c	concentration
ΔAbs	true enzymatic activity slope
$\Delta Abs_{Cal\ B}$	enzymatic activity slope
ΔAbs_{BG}	background activity slope
U_{total}	total activity of enzyme
$Y_{p\text{-}NP}$	yield of para-nitrophenol formed
$n_{p\text{-}NP}$	moles of para-nitrophenol
$n_{p\text{-}NPA}$	moles of para-nitrophenyl acetate
$V_{reactor}$	reactor volume
Q	flow rate
$A_{reactor}$	cross-section area of reactor

1. Introduction

1.1. Context of this Research

Currently, the search for sustainable and environmentally friendly alternatives in the chemical industrial sector has been growing since it can be critical to industrial achievement. It is well acknowledged that catalysis assumes an essential part in the chemical industry and industrial research field, so it can be a standpoint to minimize any harmful outcome of chemical processes. Seeking greener reactions, scientists developed outstanding approaches to satisfy financial and natural requests and the use of catalytic nanoreactors in chemical processes was seen as an imperative approach to attain chemical sustainability.

Polymeric stomatocytes are a distinguished type of nanoreactors due to having a bowl-shaped structure that results from a shape transformation induced in a polymersome. Their architecture provides an improved confinement of catalysts whether they be of metallic[10] or biological[6] nature. Polymersomes are spherical shaped hollow structures comprising a hydrophobic and a hydrophilic domain, being self-assembled from amphiphilic synthetic building blocks such as poly(ethylene glycol)-*b*-polystyrene (PEG-*b*-PS)[11][12][13], polystyrene-*b*-polyisocyanopeptide (PS-*b*-PIAT)[14] or poly(*N*-isopropylacrylamide)-*b*-poly(ethylene oxide) (PNIPAM-*b*-PEO)[15] or even biodegradable copolymers[16]. Thanks to their flexible membrane, polymersomes can acquire different morphologies[17] and therefore, via a solvent addition method reported previously[6], they can be shaped into stomatocytes. These innovative nanoparticles are capturing the attention of researchers in the field of supramolecular chemistry as they can be particularly useful for biological applications[13][16][18][19] and for catalysis applications[4][5][10][20]. However, for its use in catalysis, focus on the nanoreactor's role in protecting the enzyme and its reusability is key for efficiency, and also because there are few reports on this matter. This approach could meet the demands of "green chemistry", which poses a significant challenge to many scientists trying to make remarkable developments in the field of process chemistry and catalysis.

Candida Antarctica Lipase B (Cal B) belongs to a group of biocatalysts named lipases having many applications in the laboratory and industry. Its low cost, commercial availability and simplicity of use[21] fit the requirements of this research. Our catalytic systems should have a compartmentalized structure enhancing their utility as a nanoreactor allowing the positional assembly of Cal B in the nanoparticles. From a kinetic and thermodynamic point of view, compartmentalization within a nanoreactor is beneficial due to an increased stability and reaction rate[7] allowing structural and functional control over reaction pathways.

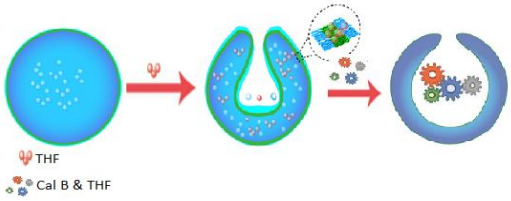

Figure 1.1- Supramolecular assembly of the biocatalytic nanoreactor via the solvent addition method.

Once the stomatocytes filled with the biocatalysts were optimized in terms of morphology and size they were tested in a continuous flow reactor setup as a nanoreactor for organic synthesis. It is well acknowledged that the use of continuous flow reactors to conduct organic synthesis allows a more accurate control over reaction parameters such as temperature and concentration as opposed to reactions conducted in batch mode, and also facilitates the scale up of the process[22]. Besides an improved control, continuous flow technology is considered a "green" technique since it contributes to a higher productivity and a low waste level along with the costs being low as well[23]. Herein an optimal method for the encapsulation of Cal B in the polymeric stomatocytes' cavities, and their performance in a flow system are reported. Finally, a milli-flow device was used as an attempt to optimize the process, as in recent years it has appeared to be a remarkable possibility in chemical reactor design[22][24]. In fact, it is well acknowledged that smaller devices improve production outcomes due to their extraordinary reaction control offering an effective homogeneity throughout the system, resulting in an improved mass transfer process[22][25][26].

1.2. Motivation and Objectives of this Research

In recent years, sustainability has gained increasing attention pushing any potential development to focus on balancing the fine line between competing needs – the need to move forward technologically and economically, and the need to protect the environment[27].

Since sustainable development has turned into a global initiative, the intersection between sustainability and chemistry has become the driving force of this research being the recovery and reusability of the nanoreactors its main concern. By trying to implement "green" techniques for chemical synthesis it is possible to reduce the generated reaction waste together with cutting costs, therefore changing the way synthetic chemistry is performed at a lab and industrial scale[23].

In this regard, the overall objective of this research is to demonstrate the potential of scaling up the applicability of nanoreactors and investigate to what extent the effects of catalyst loading and of space time can influence the performance of nanoreactors. During this research, the performance of nanoreactors was tested in a continuous flow setup. It is well acknowledged that continuous flow processing facilitates the development of sustainable manufacturing and that the selectivity provided by nanoreactors could decrease the formation of undesired byproducts and waste, both features paving the pathway to a greener process. As a way of reaching this goal, a few points are also addressed in this thesis:

i. Contextualization of the research conducted and its significance in both chemical and industrial fields;
ii. Literature review on the use of nanoreactors in the field of catalysis emphasizing the type of nanoreactors envisioned for this study and highlighting their advantages for green processing;

iii. Definition of homogeneous catalysis and how its association with Bionanotechnology can be favourable to chemical processes, thereby selecting a biocatalyst suitable for this research;

iv. Description of novel aspects within the areas of nanobiotechnology and chemical processes that should be explored in the course of this research in order to attain the main objective of this study;

v. Synthesis of stomatocytes derived from polymersomes self-assembled using amphiphilic block copolymers and encapsulation of Cal B within these polymeric vesicles, followed by their characterization using different imaging and analytical techniques;

vi. Quantification of the amount of catalyst entrapped within the nanoreactors;

vii. Determination of the effect of encapsulation on an enzyme's activity;

viii. Demonstration of important features relevant in industrial catalysis (high turnover number, use in continuous flow setup, reusability), which could make nanoreactors appealing tools in larger scale processes;

ix. Evaluation of the nanoreactors' performance in flow in terms of activity and stability by carrying out a test reaction as an attempt to optimize the system, therefore allowing process intensification as a means of potential process improvement;

x. Development of a numerical model as a way to simulate the performance of the test reaction conducted and to verify to what extent the experimental product outcome is close to the expected product outcome.

In the field of catalysis, nanoreactors are fundamental for taking the step from a lab scale to a larger scale process because they are known to offer higher productivity along with their capability of being reused which is a beneficial feature for industries. So, throughout this research the suitability of employing nanoreactors in a larger scale process was explored.

1.3. Methodology

The various steps undertaken to attain the main objective of this dissertation are sequenced in Figure 1.2 followed by a comprehensive description which can offer a clearer perception as in how it is planned to carry out this study.

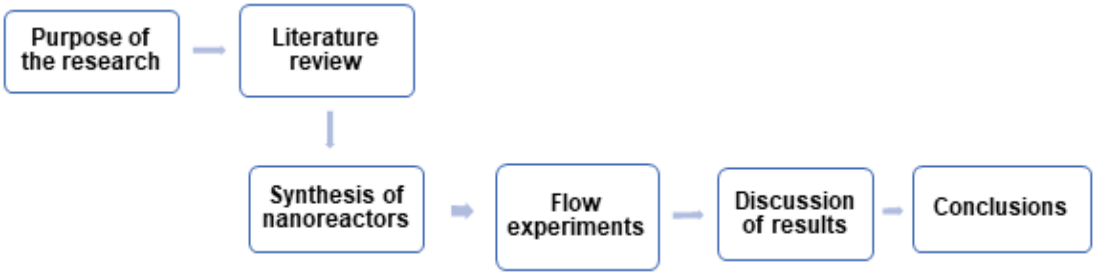

Figure 1.2- Methodology of the dissertation.

- **Step 1- Purpose of the research**

The first step taken was to explain the purpose of this research involving the employment of nanoreactors in a continuous flow process as a way to understand the substance of this study and the driving force for the work executed.

- **Step 2- Literature review**

The literature review offers an insight into the use of nanoreactors in the field of catalysis as well as a contextualization of the matter addressed throughout this research. It allows the establishment of a connection between Bionanotechnology and Catalysis which is essential to interpret the results obtained further on in this study. The theoretical background also enables to reason out and therefore introduce novel aspects to take into consideration for this research providing a guideline for the experimental procedure. This step also helps in the identification of techniques and methods that could be resourceful to obtain the necessary results.

- **Step 3- Synthesis of nanoreactors**

This step corresponds to the first phase of the experimental procedure. For the successful completion of this phase it is necessary for the nanoreactors to attain the morphology and size required, verified using various characterization techniques. The results obtained using those techniques are approved based on the literature findings. This phase also includes the verification of the effects of the enzyme's encapsulation on its kinetics.

- **Step 4- Flow experiments**

The flow experiments are part of the second phase of the experimental procedure. Once the results obtained in the first phase seem adequate, the nanoreactors can be tested in flow and their performance can be improved by setting some variables in the hopes of optimizing their overall performance in flow.

- **Step 5- Discussion of results**

The results obtained from the experimental procedure are discussed and also verified whether these findings are expected based on the literature review. The flow experiments results should be discussed from a chemical engineering perspective as to further interpret the results of the kinetic model developed.

- **Step 6- Conclusions and outlook**

This last step is intended for the conclusions made based on all the results obtained from the characterization of the nanoreactors synthesized as well as the flow experiments and the kinetic model, and also to make suggestions that could enable the field of research to progress.

1.4. Layout of the Dissertation

This Master dissertation presents the research work carried out over a course of 5 months and consists of 6 chapters. These are as follows:

- **Chapter 1** includes an overview of the purpose of this research and its contribution to the area of Industrial Catalysis and a vision of how it could possibly tackle limitations of traditional pathways. This section outlines the aim of this research.

- **Chapter 2** offers a literature review of how catalytic nanoreactors are employed in the field of catalysis focusing particularly on polymeric nanoreactors. This chapter also includes a description of the enzyme used in this study and its applications. The considerations taken into account to attain the overall goal of this research are defined allowing the identification of the key aspects to be studied, thereby presenting a clearer perspective on what is desired to accomplish throughout this research;

- **Chapter 3** gives a description of the variety of methods used for this research and how they are worthwhile to attain the results we desire. This chapter also covers the theoretical foundation behind the development of the kinetic model and presents the conditions applied to the mathematical model to predict the kinetics of the test reaction;

- **Chapter 4** concentrates on the experimental procedure on all the aspects relevant to this study. The experimental work investigates the optimization of the nanoreactors and their performance in flow by varying certain factors that were expected to have an influence over the product outcome;

- **Chapter 5** discusses the performance of the nanoreactors in flow and the extent of how the enzyme encapsulation, the catalyst load and space time can affect the product outcome. The possible limitations of these variables were discussed and a way to optimize the system was explained. The discussion of the kinetic model results includes a comparison with experimental results;

- **Chapter 6** lists the conclusions derived from this study and confirming whether nanoreactors possess a great potential for bigger scale processing;

- **Chapter 7** includes suggestions for future work aimed at improving a nanoreactor's stability and recommendations for further process intensification studies, therefore identifying a prospective direction that this research can take.

2. Theoretical Background

2.1. Nanoreactors for Catalysis

The interest in developing nanoscale chemical reactors has been rising with scientists working towards meeting the demands of “green chemistry”, which poses a significant challenge to many scientists trying to make remarkable developments in the field of synthetic chemistry. Modern chemical process technologies are willing to optimize chemical transformations by minimizing wastage and the production of undesired side products.

During the last 20 years, chemical reactor design scientists have acknowledged that “smaller means more efficient”. Using smaller volumes reduces the risk of damage to the entire system, which is able to be scaled up according to the increase in demand. Smaller reactors have a higher surface to volume ratio which results in reactions occurring mostly near the inner surface of the reactor. Interactions with a surface can bring many benefits such as improved yields caused by surface based catalysis[24], improved selectivity and increased reaction rates. These features are even more impactful when it comes to employing nanoreactors in a chemical process.

Inspired by a cell’s intricacy, a wide array of nanoreactors has been developed in the course of time to have a site-isolated catalyst system[5] through the self-assembly of small molecular components, for example, phospholipids, into capsule-containing architectures, and vesicles[28] allowing the control over the reaction pathways (higher selectivity) and also the size and morphology of the products (e.g. crystals). The aim was to enable one-pot cascade reactions through compartmentalization techniques offering a well-defined reaction environment. The cascade reactions are conducted in a way that the product of one reaction is the substrate or the catalyst of the subsequent. This sequence was envisioned by scientists as a way of increasing the efficiency of chemical conversions on scales ranging from the laboratory to an industrial process. Guided by covalent and non-covalent approaches, nanoreactors were constructed from synthetic and biological building blocks generating systems containing a cavity in which a chemical reaction can take place. While self-assembled nanoreactors’ macromolecular structures are assembled non-covalently from their building units yield robust and versatile structures, nanoreactors assembled in a covalent fashion (click chemistry [29]) involve costly multistep synthesis and are highly specific to only a limited number of reactions[28].

Most nanoreactors’ components consist of a supramolecular assembly and active compounds of biological or chemical nature encapsulated/inserted-in/attached to various regions of the assembly. These assemblies are known to retain their intrinsic properties such as their stability and robustness even though they undergo chemical modification to be combined with the active compounds. Some of the examples of nanoreactors include cage-molecules, self-assemblies from amphiphilic block copolymers, polyelectrolyte layered materials and hydrogels[24].

During the synthesis of nanoreactors, one of the main challenges is to maintain the active compound’s stability, especially in the presence of the chemicals involved (e.g. organic

solvents, and surfactants). If appropriately designed, nanoreactors can allow the encapsulation of hydrophobic as well as hydrophilic compounds contributing to the development of multifunctional systems which are needed in many fields. The outstanding feature of nanoreactors is their ability to protect the active compounds within them from environmental factors while enabling them to act *in situ*. Besides their protective nature, other characteristics are also relevant when generating nanoreactors such as the loading efficiency being adequate to support the desired application and the assembly having an adequate orientation for the facile accessibility of the substrate that supports a certain reaction. When it comes to catalysis, efficiency is a key factor and the use of nanoreactors at an industrial level can surely be beneficial as they could possibly be reused, therefore decreasing waste and consequently cutting costs.

Nanoreactors are suitable for a wide array of applications namely medicine, ecology, biotechnology and material science. This technology holds promise in the development of the "green chemistry" concept which aligns with the sustainable development goals envisioned by industries. Nanoreactors can be suitable for biochemical catalysis given their easy of synthesis, versatility in size and functionalization and their application in aqueous media.

Nanoreactors are in the early stages of development therefore they still require further intense research as a way of improving their properties to ultimately be marketable. Currently, the introduction of multifunctionality via cascade reactions as well as sustainability in chemical processes are some of the aspects researchers try to fulfil that can lead to nanoreactors that are simple, versatile, robust solutions as required today in the field of catalysis.

2.1.1. Self-assembled Nanoreactors: Polymersomes and Stomatocytes

Self-assembled nanoreactors are macromolecular structures assembled by reversible, noncovalent interactions composed by their building units[28]. Typically, such systems self-assemble through hydrogen-bonding and metal-ligand interactions. Their compartmentalization feature allows for the confinement of catalysts in their inner spaces, protecting them from any external factors. This encapsulation approach holds many advantages, specially facilitating catalyst recycling and therefore moving towards green(er) chemistry.

The use of polymers as building blocks for nanoreactors is captivating industries due to the possibility of tuning their properties[30][31] (size, polarity, stability, toxicity) thanks to their synthetic nature[7]. Nanoscience envisions combining active compounds such as proteins with synthetic materials like polymers to create functional systems therefore fusing the specificity and efficiency of the active compounds with the versatility and robustness of polymeric materials[32]. Known as macromolecular nanoreactors, these polymer nanoreactors are self-assembled using amphiphilic block copolymers built from at least two blocks with different water repellent properties that tend to aggregate amidst certain solvents dependent on the polymeric blocks thus, resembling traditional surfactants[28]. Diblock copolymers are formed when a hydrophilic block is connected to a hydrophobic block through polymerization techniques such as Atom Transfer Radical Polymerization (ATRP) or Reversible Addition Fragmentation Chain-Transfer (RAFT) polymerization. The hydrophobic block is typically based on polystyrene (PS),

polybutadiene or poly(dimethylsiloxane) (PDMS), whereas the hydrophilic block is usually poly(acrylic acid) (PAA), polyethyleneglycol (PEG), polymethyloxazolidine (PMOXA), or poly(*N*-hydroxypropyl)methacrylamide (PHPMA)[32]. Micellar, bilayer and chiral morphologies are some of the resultant architectures of amphiphilic block copolymers dispersions. The morphologies generated are dependent on the length of the polymer block and the ratio of the hydrophobic and hydrophilic blocks. Micelles prevail when the hydrophilic block is predominant (over 50%), 40–50% leads to rod-like structures, whereas polymeric vesicles are formed at 25–40%. The minimum size of the supramolecular assembly (micelles or vesicles) is restricted by the membrane's maximum curvature determined by the ability of a single amphiphilic copolymer molecule to adopt a conical shape[33]. The driving force for the self-assembly is assumed to be the microphase separation of the insoluble blocks.

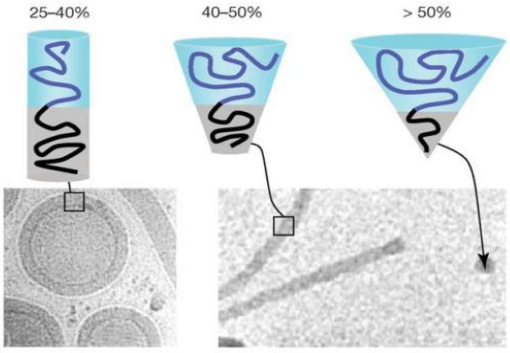

Figure 2.1- Relation between polymer block length and the structure of the polymeric supramolecular assembly with respective cryo-TEM images showing vesicles or tube and spherical micelles. Blue portion: hydrophilic block; Black portion: hydrophobic block[33].

Polymeric vesicles also called polymersomes are spherical compartments self-assembled from amphiphilic synthetic block copolymers such as poly(ethylene glycol)-*b*-polystyrene (PEG-*b*-PS), polystyrene-*b*-polyisocyanopeptide (PS-*b*-PIAT) or poly(*N*-isopropylacrylamide)-*b*-poly(ethylene oxide) (PNIPAM-*b*-PEO) in dilute aqueous solutions given their low critical micelle concentration[34]. Their microenvironment is comprised of an aqueous lumen and a hydrophobic membrane[7] thus serving as hosts to hydrophilic molecules (e.g. enzymes) inside their cavities and to hydrophobic molecules (e.g. metal catalysts) in their membranes- dual carrier role- and their size ranges from 50 to 400 nm[32].The hydrophobic

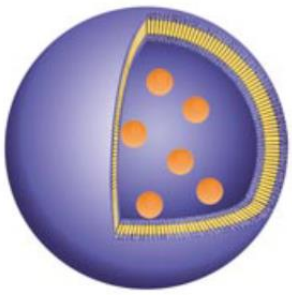

Figure 2.2- Polymeric nanoreactor used for encapsulating active compounds. Orange spheres: active compounds[32].

blocks of each molecule tend to associate with each other therefore minimizing direct exposure to water, whereas the more hydrophilic blocks face inner and outer aqueous solutions thereby delimiting the two interfaces of a bilayer membrane[33]. It is important to ensure that a polymer assembly is permeable enough to allow penetration of the substrate that supports a certain reaction.

Polymersomes resemble liposomes due to the similarity between the building units used to generate these structures and, consequently, they possess similar amphiphilicity. However, liposomes' efficacy is diminished due to poor stability and leak-tightness[35], while polymersomes possess greater chemical and physical stability resulting from the low entropy of the mixing of polymers[32], making them excellent candidates for nanoreactor applications[1]. Polymer vesicles' assembly process is slower and a thicker membrane is formed[35], assuring them a higher mechanical stability compared to liposomes.

Polymersomes are intriguing nanostructures because by changing the chemical nature of their building blocks, or the active compound(s) combined with them, they can be suitable for applications in catalysis or in drug delivery. They hold promise for catalytic processes heading towards green(er) processing, because they are capable of protecting the catalyst as well as enabling their recyclability, property that is often speculated. Besides this, the execution of incompatible cascade reactions is possible within polymersomes given their catalyst compartmentalization and positional methodology. The use of water as a reaction medium is possible when using site-isolated techniques (e.g. nanoreactors) to perform asymmetric catalysis using chiral catalysts[7][20] which are incompatible with aqueous solutions. Polymer nanoreactors are known to improve catalytic activity and also offer higher yields and selectivity thanks to their high surface to volume ratio[36] allowing rapid diffusion of the substrate into the enzyme's active sites.

It is well acknowledged that the morphology and size of the polymersomes are under the influence of the copolymer chemistry, solution composition and environmental conditions. Via an osmotic pressure mediated process, liposomes can be shaped into several non-spherical architectures such as oblates, prolates and stomatocytes[36]. The same approach can also be applied to polymersomes due to the similar amphiphilicity of their building units as previously mentioned. Stomatocytes are bowl shaped vesicular structures with an "opening" connecting the "stomach" to the outer environment capable of encapsulating enzymatic networks contributing to the formation of complex nanoreactors and nanomotors[6][10][16]. This procedure has been demonstrated for polymersomes assembled from polystyrene-based copolymers, such as poly(acrylic acid)-*block*-polystyrene (PAA-*b*-PS) and poly(ethylene glycol)-*block*-polystyrene (PEG-*b*-PS)[12]. It was found that the use of organic solvents (e.g. THF/dioxane) as plasticizing agent is essential since it will provide enough mobility and permeability to the PS membrane which will undergo a phase transition state from a solvent swollen rubbery state to a rigid glassy state[35], therefore vitrifying the structures into out-of-equilibrium shapes like stomatocytes. When the shape transformation procedure is performed in the presence of

catalytic species, they become engulfed in the stomatocyte's cavity and once its opening is sealed the catalysts are well confined within the stomatocyte[6][36].

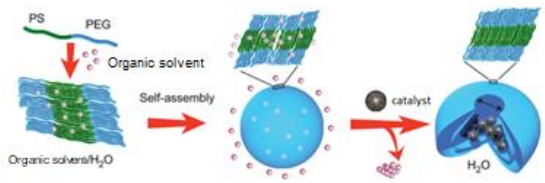

Figure 2.3- Preparation of catalytic polymeric stomatocytes: after formation in a mixture of water and organic solvent, addition of water leads to the formation of spherical polymersomes and further catalyst encapsulation[36].

The search for a detailed understanding of the correlation between the structure and the function of nanoreactors is still ongoing and a better scope into the molecular processes that take place within them continues under research. However, the field of nanoreactor science and engineering is flourishing as a result of their unifying aspect being their overall positive impact on chemical processes by influencing the kinetics and thermodynamics of the reactions.

2.2. Catalysis in Bionanotechnology

Bionanotechnology has the potential of providing cheaper and effective manufacturing with environmental mindfulness that can facilitate progress towards process development goals of sustainability and production patterns[37][38]. Therefore, linking biocatalysis with nanotechnology can ensure a neater and more efficient chemical process as compared to traditional standards.

Catalysis is defined as homogeneous when the reactants and catalysts are dissolved in the same phase (usually a liquid phase). Homogeneous catalysis involves the use of biocatalysts (enzymes), organocatalysts and metal catalysts[7].

Homogeneous catalysts present a high degree of dispersion resulting in more collisions with substrate molecules. As a result, the substrate molecules are not hindered from reaching the catalytic active sites from any direction and that being so, the use of a low catalyst concentration and mild reaction conditions are suitable for performing homogeneous catalysis. Kinetic control is more prominent for reactions catalyzed by homogeneous catalysts compared to diffusion control, because a facile mass transport between the substrate and enzyme is evident[39].

Although this type of catalyst can offer better conversions and higher selectivity[40] it is under the risk of deactivation due to physical and chemical processes since they require some sort of protection. This is where nanoreactors can play an important role on preserving their activity by shielding and segregation of the catalyst used for the reaction. Beside this, nanoreactors can ease their separation from the reaction medium after the reaction takes place[41]. Polymersomes have been most often used as biocatalytic nanoreactors[7][42].

Biocatalysts (enzymes) present improved thermostability, tolerance to acid, base and/or organic solvents, and reduce substrate or product inhibition, resulting in remarkable activities and selectivities by being able to optimize for near total stereo- or regio-selectivity for a desired product[43], making them attractive candidates for catalyzing chemical processes preferable for large scale manufacture. Most enzymes operate under mild conditions such as at room temperature, neutral pH and at low concentrations[44].

The hope of increasing the separability of the homogeneous catalysts stem from requirements for applications on an industrial level. Once this feature is improved, complicated processes such as distillation, liquid-liquid extraction and ion exchange[39] for catalyst recovery can be forgone.

2.2.1. Candida Antarctica Lipase B

Candida Antarctica Lipase B also known as Cal B is the enzyme used to catalyze the hydrolysis reaction used in this research and it comes under the widely used group of biocatalysts named lipases. Lipases are one of the few enzymes that can catalyze synthetic reactions under a water restricted environment and hydrolysis reaction under aqueous conditions[44].

In terms of structure, lipases usually have a protein loop (lid) which covers the enzyme's active site. However, conformational change in the lid converts the enzyme from closed (inactive) to open (active) form exposing the hydrophobic residues thus, increasing the apolarity around the active site and stabilizing the interaction with substrate interface[44]. The described mechanism corresponds to a phenomenon called interfacial activity and it can cause a significant increase in catalytic activity. However, this feature is variable, some lipases can possess two lids, while others have no lid and show no interfacial activity[45].

Lipases are defined as carboxylesterase, enzymes that catalyze hydrolysis reaction and synthesis of long chain acylglycerols. They are widely used for biotechnological applications due to displaying attractive properties such has great regioselectivity and stereoselectivity and they can be produced from microbial organisms. Besides these features, they do not require a cofactor like most enzymes do hence, easing their application.

Particularly, Candida Antarctica Lipase B (Figure 2.4) belongs to the enzyme class of hydrolases and it acts on ester bonds of carboxylic esters[21]. With this in mind, the test reaction selected for this research was the hydrolysis of p-nitrophenyl acetate (Figure 2.5) since the latter is classified as a carboxylic ester. This enzyme is not considered a true lipase due to not possessing interfacial activation, like most of them do, since the lid structure covering the active site seems to be absent or very small[44]. Cal B possesses an oxyanion hole that stabilizes the transition state in the reaction intermediate. The active site contains a small cavity called a stereospecificity pocket in which secondary alcohols have to orient one substituent during catalysis. This offers Cal B a high enantioselectivity towards chiral secondary alcohols.

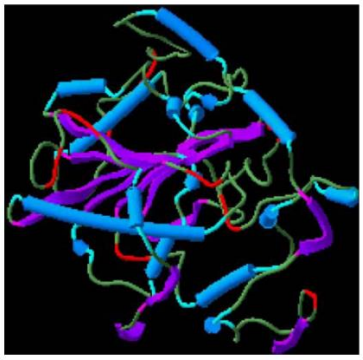

Figure 2.4- Candida Antarctica Lipase B structure[44].

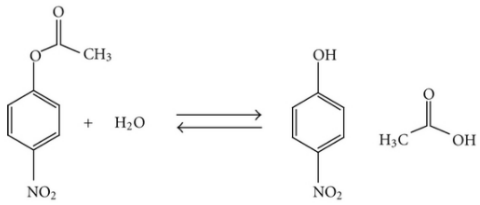

Figure 2.5- Test reaction: hydrolysis of p-NPA to p-NP.

Cal B is one of lipases which has many applications in the laboratory and in the industry. In the industry it is used for the production of detergents, for biodiesel and for various types of fermentations[46]. This lipase comes across as an appealing biocatalyst due to its simplicity of use, low cost and commercial availability[21]. However, their use in industrial processes is still limited by their unreliable stability under operational conditions and difficult separation from reaction mixture which translates into a need for process intensification for Cal B for continuous processing by testing its performance in a smaller scale reactor[47][48]. The need for process intensification of Cal B turned into one of the guidelines of this research in the hopes of improving its activity, stability and reusability.

2.3. Considerations for Scaling Up the Applicability of Nanoreactors

In recent years, industries are broadening the scope of applications of enzymes since they are known to offer competitive processes[49]. Although enzymes seem to be attractive tools for catalysis they present shortcomings in terms of stability and recovery. Once Bionanotechnology and industrial catalysis intersected, the concept of nanoreactors emerged and was seen as revolutionary as they could possibly overcome the limitations imposed when using biocatalysts in chemical processes. Actually, Feynman in 1959 stated that endless possibilities in science and in industries could surface once manipulation of matter at a nanoscale was feasible[50][51] and now, nanoreactors serve as proof.

Advancements in nanoscale science have led to the developments of novel materials and outstanding techniques which are affecting production outcomes in various manufacturing industries[51]. Self-assembly is perceived as a technique that makes products by assembling

them “bottom-up” from individual atoms. Following this technique, a nanoreactor is assembled and prepared to be used for catalytic applications.

This research was aimed to demonstrate some important features pertaining to industrial catalysis which could make nanoreactors appealing tools for large scale processes such as the improvement of kinetic properties when the enzyme is encapsulated, use of the nanoreactors in a continuous flow setup and to what extent their reusability can affect the enzyme’s activity. The mentioned features and their relevance to industries were outlined in the following sections.

2.3.1. Enzyme Kinetics

The use of enzymes as biocatalysts has gained popularity in recent years, particularly in chemical, pharmaceutical and bio-industrial manufacturing and in the environmentally friendly developments, therefore examining enzyme kinetics is critical for using them in industries[52]. However, one of the major hurdles to application of enzymes in synthetic chemistry is their inadequacy to withstand wide fluctuations in process conditions, the exposure to solvents and non-physiological temperatures and pH values[53], which can force process engineers to alter process parameters[54], which is not plausible. To overcome these issues, researchers aim to improve the enzyme’s properties and performance to suit the needs of industrial use. With the advent of nanoreactors, an enzyme confined within their inner space could possibly preserve its activity due to nanoreactors being capable of shielding enzymes from environmental factors. The question then arises as to whether an enzyme’s kinetic properties are diminished or improved in a way that could be meaningful for the manufacturing process when employed in its encapsulated form.

For over a century, the Michaelis-Menten equation has been widely used to estimate the enzyme kinetic parameters from reaction progressive curves of substrate consisting of a canonical approach[52]. This equation describes a hyperbolic relationship between initial velocity and substrate concentration for a system where a substrate S binds reversibly to an enzyme E to form an enzyme-substrate complex ES, which then reacts irreversibly to form a product P and to regenerate the enzyme E.

$$E + S \rightleftharpoons ES \rightarrow E + P$$

The scheme for derivation of the Michaelis-Menten equation was described by George Briggs and J.B.S. Haldane in 1925 and it can be represented as follows:

$$E + S \underset{k_{off}}{\overset{k_{on}}{\rightleftharpoons}} ES \xrightarrow{k_{cat}} E + P$$

The rate constants included in this scheme are k_{on} representing the bimolecular association of the enzyme-substrate binding and k_{off} stands for the dissociation of the ES complex to regenerate the enzyme and substrate and k_{cat} represents the dissociation of the ES complex to give enzyme and product P.

The rates of change of all the chemical species involved based on a steady-state approximation are given as follows:

$$\frac{d[S]}{dt} = -k_{on}[E][S] + k_{off}[ES] \quad (1)$$

$$\frac{d[E]}{dt} = -k_{on}[E][S] + \left(k_{off} + k_{cat}\right)[ES] \quad (2)$$

$$\frac{d[P]}{dt} = k_{cat}[ES] \quad (3)$$

$$\frac{d[ES]}{dt} = k_{on}[E][S] - (k_{off} + k_{cat})[ES] \quad (4)$$

The steady-state assumption is valid if an initial velocity assay (initial rate analysis) is studied to estimate the kinetic parameters. For this assay, initial rates of the reaction are calculated for a range of substrate concentrations followed by the use of a linear (Lineweaver-Burk plots) or second order polynomial fitting of the enzymatic data obtained, the parameters can be easily estimated. To ensure the kinetic parameters are identified appropriately it is important that the initial substrate concentration is increased from a low level to a higher level so that the enzyme molecules are saturated by substrate molecules[52]. Since this research uses the initial velocity assay to compare the enzyme's kinetic properties when it is in its free form and in its encapsulated form, it is acceptable to assume that [ES] is constant:

$$\frac{d[ES]}{dt} = 0 \quad (5)$$

$$k_{on}[E][S] = \left(k_{off} + k_{cat}\right)[ES] \quad (6)$$

To calculate [ES] the equation above is rearranged knowing that the enzyme concentration in its initial form [E] is equal to the total enzyme concentration [E_T] minus the concentration of enzyme-substrate complex [ES].

$$k_{on}([E_T] - [ES])[S] = \left(k_{off} + k_{cat}\right)[ES] \quad (7)$$

$$k_{on}[E_T][S] - k_{on}[ES][S] = (k_{off} + k_{cat})[ES] \quad (8)$$

$$k_{on}[E_T][S] = \left(k_{off} + k_{cat}\right)[ES] + k_{on}[ES][S] \quad (9)$$

$$[ES] = \frac{k_{on}[E_T][S]}{(k_{off}+k_{cat})+k_{on}[S]} = \frac{[E_T][S]}{\left(\frac{k_{off}+k_{cat}}{k_{on}}\right)+[S]} \quad (10)$$

$$v = k_{cat}[ES] = \frac{k_{cat}[E_T][S]}{\left(\frac{k_{off}+k_{cat}}{k_{on}}\right)+[S]} \quad (11)$$

Since V_{max} is the maximum rate achieved at a saturating substrate concentration, it is equal to k_{cat}[ES] when [ES]=[ET] and it is related to the efficiency of a reaction catalyzed by a certain enzymatic species.

$$V_{max} = k_{cat}[E_T] \quad (12)$$

$$K_M = \frac{k_{off}+k_{cat}}{k_{on}} \quad (13)$$

Finally, the Michaelis-Menten for this system is described as:

$$v = \frac{V_{max}[S]}{K_M+[S]} \quad (14)$$

The rate constant k_{cat}, is related to the number of molecules of product generated by an enzyme in a specified period of time known as "turnover number". In industrial catalysis, k_{cat} is

usually described as “turnover frequency” and it refers to the number of product molecules formed before the inactivation of the catalyst. It is a very important enzymatic feature to take into account since it can avoid an engineer having to suddenly halt a process due to having to replace the catalyst[55]. The Michaelis-Menten constant, K_M, provides an estimation of the affinity of the enzyme for a substrate.

By studying the Cal B’s intrinsic kinetic properties, whether in its free or encapsulated form, when catalyzing the hydrolysis of p-nitrophenyl acetate to p-nitrophenol provides a better insight on its suitability for large scale processes and can even lead to process improvements from a commercial point of view as well.

2.3.2. Continuous Flow Processing

Previously, batch reactors were used to conduct all chemical reactions. However, from a process chemistry perspective, a major drawback is witnessed when it comes to batch technology being it the failure to scale up successful reactions, since it would demand the redevelopment of synthetic routes which could be a time consuming and costly procedure[22]. As an attempt towards increasing the ”green” prospects of chemical manufacturing processes and as a means of keeping productivity high and costs low, continuous processing was considered as one of the key areas for research activities[23].

Continuous flow technology provides an accurate control over reaction parameters, such as the regulation of temperature and concentration, which are crucial for product selectivity and ensure a safe process. An excellent heat and mass transfer are also verified leading to a better reaction control compared to batch technology. Despite the advantages associated with flow systems, there was a need for process improvement to meet the increasing demands of sustainable production. As a result, the concept of process intensification was put into practice as an approach to comply with the needful requirements, since it could ideally allow the direct use of a continuous process developed in lab-scale as the commercial scale process. Miniaturized devices are essential tools for the implementation of process intensification[56].

The use of smaller scale reactors is beneficial due to the higher surface to volume ratio which permits a rapid heat exchange and mass transfer. It is well acknowledged that transport phenomena dictates a reaction’s performance since transport coefficients are typically inversely proportional to the characteristic dimension of the system so reducing the size of chemical systems leads to a substantial increase in transport rates. This increase leads to the enhancement of the overall rate of processes that are transport limited[57] favoring yield and selectivity. The smaller diffusion path has been considered as a major driving force for process intensification[56].

Mass transfer is a relevant property when it comes to employing the nanoreactors in a continuous flow setup and it is dependent on the catalyst present within these structures as well as on the reaction time. Flow experiments, based on the hydrolysis of p-nitrophenyl acetate to p-nitrophenol, were conducted in milli-flow devices to decide the optimum conditions under which the Cal B nanoreactors synthesized can be employed in terms of catalyst load, and the

effect of space time was studied as an attempt to optimize the system with the intent of obtaining a maximal throughput.

Factors like physical properties of the dispersion or micromixing are important for mass transport and reaction applications. Dispersion occurs due to variations in the velocity profile of the fluid which passes through the reactor and results in fluid elements exiting the reactor at different residence time, which can influence the final conversion at the reactor exit. Micromixing is defined as the mixing degree on a molecular scale. Achieving stable flow patterns result from the balance of inertial, viscous and interfacial forces. A combination of dimensionless numbers measure the importance of these features at the milli-scale. The Reynolds number, Re, is the ratio between inertial forces and viscous forces, and can serve to predict whether the flow will be laminar (Re<2000) or turbulent (Re>3500), being defined by:

$$Re = \frac{\rho u D}{\mu} \tag{15}$$

where ρ if the fluid density, u is the flow velocity, D is the characteristic length, which, in this case, is equivalent to the internal diameter of the reactor and μ is the dynamic viscosity. In the context of mass transfer, the Peclet number is also relevant and it is defined by the rate of forced convention to diffusion:

$$Pe = \frac{uL}{D} \tag{16}$$

where u, L and D denote the average linear velocity through the tubular reactor, the transverse diffusion distance and the dispersion coefficient, respectively[58]. The Peclet number for mass dispersion is often referred to as the Bodenstein number[59], Bo, in reacting systems so:

$$Bo = \frac{uL}{D_{ax}} \tag{17}$$

where u is the linear flow rate, L is the effective length of the reactor and D_{ax} is the axial dispersion coefficient. Micromixing is characterized by the Damkőhler number and verifies whether the overall process is limited by the reaction time or by the transport time of the species involved in the reaction and it is defined by:

$$Da_M = \frac{\tau_t}{\tau_r} \tag{18}$$

where τ_t and τ_r are the transport time and the reaction time, respectively[56][60]. Three regions of mixing are identified: Da_M<0,001, the reaction becomes kinetically controlled, Da_M>1000 reaction limited by mixing and 0,001<Da_M<1000 both reaction kinetics and mixing are important. These dimensionless numbers offer a true insight into the influence of mixing and flow behavior in a reactor setup for a reactor performance comparison.

Linking biocatalysis to flow technology widens the scope of this research offering different solutions for chemical and bio-chemical issues, with the underlying goal to enhance the selectivity and yield of reaction through the use of nanoreactors.

2.3.3. Reusability of Nanoreactors

Enzymatic reactions and continuous flow methodologies have come together as a result of industrial attempts to improve existing processes due to enzymes presenting great potential compared to chemical catalysts. This coupling brings some benefits, including reproducibility and minimized waste generation[54]. Nevertheless, as pointed out before, some challenges are persist, such as the reusability of the enzyme when employed in flow along with preserving its activity, an area in which the applications have so far been sporadic.

This research envisioned to synthesize selective nanoreactors permitting potential reuse and effectively proving that nanoreactors are outstanding in terms of protecting the enzyme encapsulated within them. To demonstrate one of the main advantages of using a nanoreactor, leaching experiments were performed by reusing the nanoreactors and monitoring their activity after each cycle of reuse. The main concern was to show that the nanoreactors tend to lose activity due to losing enzyme molecules and are not affected by the flow configuration, thereby confirming their protectiveness. The variable for this set of experiments was the catalyst load since it is important to verify if the extent of the loss in activity is related to the amount of catalyst confined in the supramolecular assembly.

Owing to the scientific advancements in enzyme engineering as well as economic pressure, reusability of an enzyme is considered an important factor at an industrial scale. The prospect of employing nanoreactors in flow coupled with their reusability could bring biocatalysis a leap closer to sustainable manufacturing.

3. Methods

3.1. Characterization Methods for Biocatalytic Polymeric Vesicles

The characterization of nanoreactors from a structural point of view involves a complex scheme of analytical methods. It is important to evaluate their size and morphology as well as their stability upon assembly.

3.1.1. Light Scattering

Light Scattering was the method of choice to determine the average diameters, the polydispersity and to assess the specific morphology of the polymer assemblies[32][61]. In particular, Dynamic Light Scattering was used to determine these properties and the results have been discussed further in this thesis.

3.1.1.1. Dynamic Light Scattering

Dynamic Light Scattering (DLS) also known as Photon Correlation Spectroscopy (PCS) or Quasi Elastic Light Scattering (QELS) is a non-invasive, well-established technique for measuring the size distribution of molecules and particles. This method monitors the time-dependence fluctuations of the intensity of light scattered by the medium measured by a fast photon counter[62][63].

DLS measures the speed of particles undergoing Brownian motion which is defined by the random movement of particles caused by the bombardment by the solvent molecules that surround them. It is acknowledged that small particles diffuse rapidly as opposed to large particles since their Brownian motion is faster. A stable temperature is required for DLS to avoid non-random movements caused by convection currents in the sample, therefore misinterpreting the size of the particles.

The velocity of the Brownian motion is defined by the translational diffusion coefficient (D) that can be converted into a particle size using the Stokes-Einstein equation,

$$d_H = \frac{kT}{3\pi\eta D} \quad (19)$$

where d_H is the hydrodynamic diameter, k is the Boltzmann's constant, T is the absolute temperature, η is the viscosity and D is the translational diffusion coefficient. The diameter obtained corresponds to the diameter of a hard sphere that diffuses at the same speed as the particle being measured. It will be dependent on any surface structure, on the shape and as well as on the concentration and type of ions in the medium. The conductivity of a medium can influence the diffusion speed by changing the thickness of the electric double layer called the Debye length[64]. For example, a smaller hydrodynamic diameter would be obtained for a particle suspended in a salt solution than for a particle suspended in deionized water.

Figure 3.1 represents a scheme with the different DLS instrument components. According to this scheme, a laser is passed through the particle sample and as a result the particles will scatter light at all angles. The majority of instruments measure the light at an angle

of 173º to the laser beam (backscatter detection). The detector used is capable of counting individual photons and the signal produced will be the number of photons detected as a function of time. The rate of fluctuation of the scattering intensity is determined by the particle size. The fluctuations in intensity are due to billions of particles undergoing random diffusion and since they are not stationary an average intensity is detected which fluctuates over very short time scales. The signal produced will pass through a digital signal processor (correlator) where the time analysis is carried out.

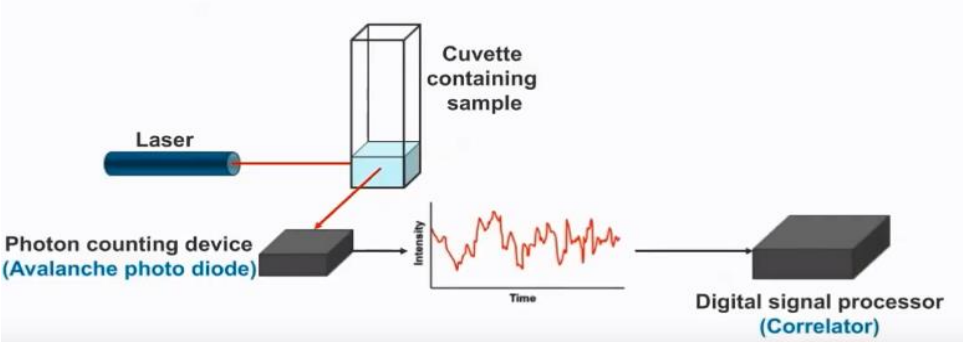

Figure 3.1- DLS instrument components.

Correlation in Dyanmic Light Scattering is a technique for extracting the time dependence of a signal in the presence of "noise". The correlator will construct a correlation function G(τ) of the scattered intensity according to:

$$G(\tau) = \langle \frac{I(t_0) \times I(t_0+\tau)}{I(t_\infty)^2} \rangle \quad (20)$$

where I is intensity, t is the time and τ is the delay time. For large number of monodisperse particles in Brownian motion, the loss of correlation is an exponential process which results in the exponential decay rates in correlation of the function of delay time given by:

$$G(\tau) = A[1 + Bexp(-2\Gamma\tau)] \quad (21)$$

where A is equal to the baseline of the correlation function and B s the intercept of the correlation function and $\Gamma = Dq^2$, $q = (4\pi n/\lambda_o)\ \sin(\theta/2)$ where n, λ_o and θ denote the refractive index of dispersant, wavelength of the laser and the scattering angle, respectively[64].

The dispersity index (Đ = M_w/M_n) related to the size distribution of the macromolecules is also measured by the DLS. The recommended PdI value for self-assemblies is below 0,5 since a high degree of order should be attained. This index along with the size distribution by intensity of light scattered by the medium obtained reveals the existence of morphology polydispersity. This indicates whether it is needed to resort to methods used to isolate the desired structures such as size exclusion chromatography (SEC), filtration or extrusion.

3.1.2. Electron Microscopy

Transmission Electron Microscopy (TEM) and Scanning Electron Microscopy (SEM) are the methods of choice to obtain information regarding the morphology and size distribution of

the polymeric nanoreactors. They offer an outstanding depth of field and a high degree of magnification.

The high resolution of electron microscopy (EM) images results from the use of electrons as the source of illuminating radiation. The things that are seen to human beings are determined by the light that shines through them, for example an ordinary light microscope uses photons as light equivalent to waves with a wavelength of 400 to 700 nm, but to view things that are really tiny like bacteria (200 nm) or proteins (10 nm) researchers need to resort to particles possessing an even shorter wavelength than photons. The use of electrons is adequate as an illumination source which means that a stream of electrons takes the place of a beam of light[65].

A transmission electron microscope fires a beam of electrons through a specimen to produce a magnified image of an object, while a scanning electron microscope scans a beam of electrons over a specimen to produce a magnified image of an object. The SEM image is inverted compared to the TEM. Bright areas of the image are the result of more electrons being scattered.

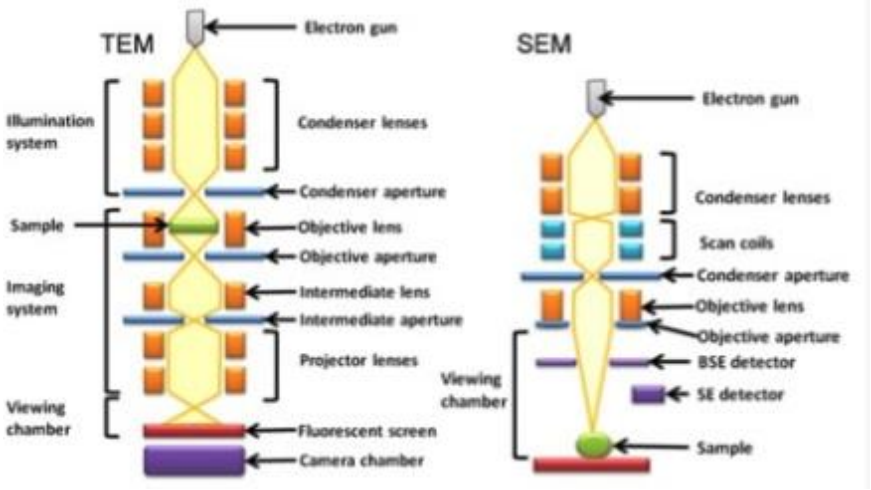

Figure 3.2- The optics of a transmission electron microscope and scanning electron microscope[66].

Figure 3.2 represents both TEM and SEM microscopes. As it is seen, both types of electron microscopes have an electron gun containing an electron source, a Wenhelt cylinder to form the beam and an anode to accelerate the beam. The three main types of electron sources are the tungsten filament, a lanthanum hexaboride (LaB_6) crystal and a field emission filament and they differ in brightness, energy range and resolution.

Of these methods, TEM has the added advantage that allows the dimensions and shape of the nanoreactor interior space to be seen while SEM generates a topological image of a sample, therefore it can be used to verify if the nanoreactor presents a bowl-shaped structure (stomatocytes) and make sure whether the catalyst is effectively encapsulated within the inner space of the polymeric assembly.

3.1.3. Assymetric Flow Field-Flow Fractionation

Asymmetric Flow Field-Flow Fractionation (AF4) is an analytical separation technique used for the characterization of nanoparticles, polymers and proteins. The high-resolution separation is achieved solely within a flow in an empty channel where a perpendicular flow force is applied. The channel consists of two plates bolted together separated by a spacer foil. The upper channel plate is impermeable, while the bottom plate is permeable covered by a semipermeable membrane with a typical size barrier of 5 to 10 kDa to prevent the sample from penetrating the channel and directs it by flow to the channel outlet. The laminar flow of the mobile phase creates a parabolic flow profile within the channel.

The sample particles are driven by the cross flow towards the bottom plate also known as the “accumulation wall” of the channel. As these particles reach this boundary layer they undergo a counter acting diffusion against the cross flow causing smaller particles, which have a higher diffusion coefficient, tend to move closer to the channel center, where the longitudinal flow is faster. The velocity gradient observed inside the channel (Figure 3.3) separates particles according to their size so that the larger particles move towards the channel outlet with a lower velocity and elute later than the smaller particles[67].

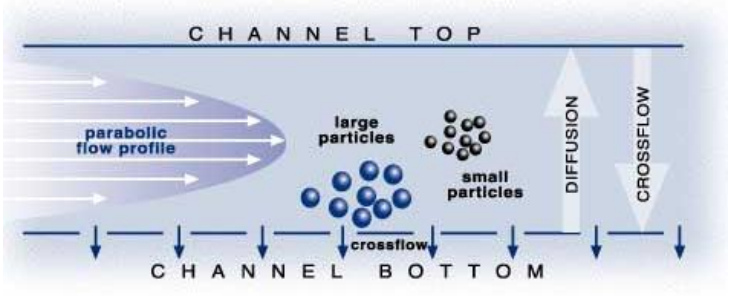

Figure 3.3- Influence of the separation field in AF4.

This technique is used to verify if there is any enzyme residue stuck to the outer surface of the stomatocyte and can prove whether the enzyme is confined within the inner space of the polymeric assembly or seeping out of it.

3.2. Enzymatic Quantification and Activity Measurement Techniques

3.2.1. Spectrophotometric Assay

A spectrophotometric assay based on hydrolysis of p-NPA was conducted to measure the activity and quantitative analysis of Cal B in the polymer assembly by monitoring the formation of p-NP. Besides this, a kinetic study is also performed using this procedure to verify the effect of encapsulation on Cal B’s activity, by estimating the kinetic properties of the free enzyme and after its encapsulation using the Michaelis-Menten equation.

A spectrophotometer measures the intensity of light absorbed after passing through a sample solution. It consists of a spectrometer and a photometer. A spectrometer produces a

desired range of wavelength of light. For the assay conducted, it is known that the product, p-nitrophenol, has the maximum absorbance at approximately 405 nm so light at this wavelength is transmitted to pass through the sample solution in the plate reader. The number of photons absorbed by the solution is detected by the photometer and then the signal is sent to the readout device (Figure 3.4).

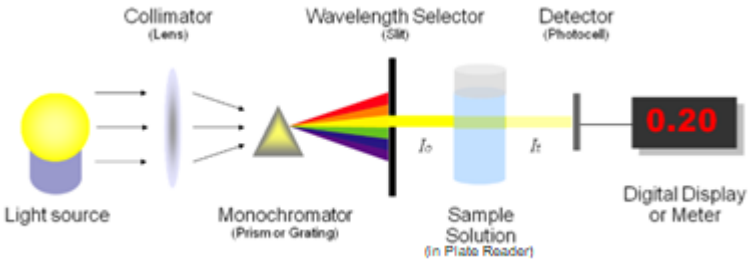

Figure 3.4- Basic structure of spectrophotometers.[68]

The number of photons that pass through the well in which the sample is placed and then into the detector is proportional to the path length of the well and the concentration of the sample. In a spectroscopy experiment, transmittance is the parameter measured which refers to the fraction of light that is able to pass through the sample calculated by:

$$Transmittance(T) = \frac{I_t}{I_0} \quad (22)$$

where I_t corresponds to the light intensity after the beam of light passes through the well and I_0 is the intensity of incident light. Since transmission decays exponentially with the increase of enzyme concentration, absorbance is more practical because it shows a linear increase with concentration and it is related to transmittance by the expression:

$$Absorbance\ (Abs) = -\log(T) = -\log\left(\frac{I_t}{I_0}\right) \quad (23)$$

where absorbance stands for the amount of photons absorbed. The unknown concentration can be determined resorting to Beer-Lambert law, where absorbance is linearly related to the concentration of enzyme in the sample:

$$Abs = \varepsilon lc \quad (24)$$

where Abs, ε, l and c denote the absorbance, the molar absorptivity, the path length and the concentration, respectively.

3.2.2. Bradford Assay

The Bradford protein assay is a quantitative assay used to determine the total protein concentration of a sample. The principle of this assay is based on the binding of Coomasie Brilliant Blue (Figure 3.5) to protein molecules under acidic conditions resulting in a color change from brown to blue. The special feature that is useful for the Bradford assay is that Coomassie Blue exists in two states: cationic (unstable) and anionic (stable).

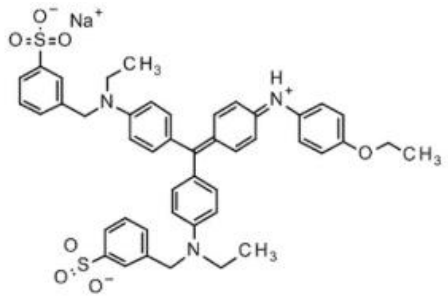

Figure 3.5- Coomasie Brilliant Blue dye molecule.

To know the concentration of a protein in a solution, a sample of protein solution is mixed with the Coomassie Brilliant Blue dye in its unstable state (brown color) in an acidic medium. Protein molecules are usually positively charged under acidic conditions. The lone electron pair of the dye molecule can be given to the existing ionizable groups of the protein molecule therefore destabilizing it. Since the unstable protein is positively charged and the unstable dye molecule is negatively charged they bind together thanks to ionic forces. The bond is reinforced due to Van der Waals hydrophobic forces due to the nonpolar region of the Coomassie Brilliant Blue and hydrophobic pockets in the tertiary structure of the unstable protein. The protein-dye complex formed is stable, thereby also stabilizing the Coomassie blue confirmed by the solution turning blue.

The dye in its unstable state absorbs light at 465 nm. On the other hand, in its stable state it absorbs light at 595 nm meaning the higher the absorbance at 595 nm, the bluer the solution and therefore there is a higher protein concentration in the solution[69]. To measure the concentration of protein, a calibration curve is needed. Several dilutions of Bovine Serum Albumin (BSA) are made starting from a known concentration and added to the dye. The absorbance of the solutions is measured at 595 nm in the spectrophotometer and the standard curve is built, which helps to obtain the unknown protein concentration of the sample.

3.2.3. SDS-PAGE

SDS-PAGE (sodium dodecyl sulfate-polyacrylamide gel electrophoresis) is an analytical method that can yield information regarding a protein's size (molecular weight) and quantity with the aid of image analysis software. This technique was used to quantify the amount of Cal B internalized in the polymeric assembly.

This separation technique is based upon the principle that a negatively charged molecule will migrate in an electric field towards an electrode with an opposite sign. For this to happen, protein samples are loaded into wells and electric voltage is applied. A reducing agent such as mercaptoethanol or dithiothreitol (DTT) breaks down the disulfide bridges (S-S bridges) that are responsible for the secondary structure of the proteins, leaving them with their primary structure. This also occurs in the presence of a detergent such as SDS, which binds covalently to proteins, causing their denaturation, and imparts a negative charge to the proteins evenly, thereby linearizing them into polypeptides. This way macromolecules get separated on the basis of size and not on the basis of shape or charge. The polyacrylamide gel provides a matrix

for electrophoretic mobility. The negatively charged polypeptides run towards the positive electrode (anode) through the gel once an electric field is applied and are separated by a molecular sieving effect based on size[70][71], as illustrated in Figure 3.6.

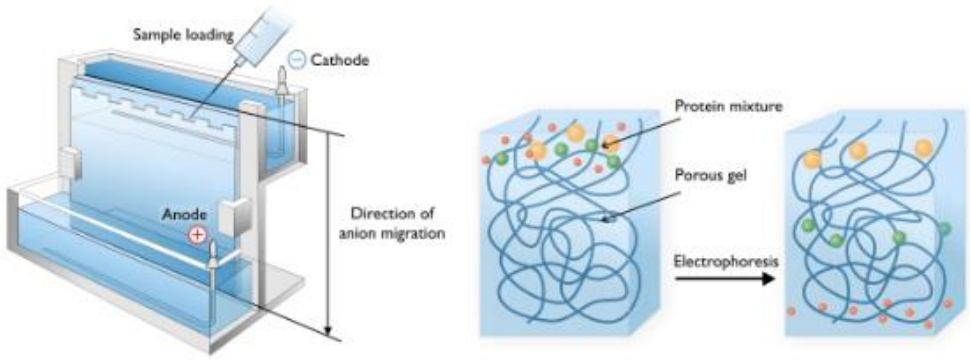

Figure 3.6- Separation of proteins in a polyacrylamide gel[72].

Once protein bands have been separated by electrophoresis they can be analyzed using different staining techniques[73]. The most common staining method is the one involving Coomasie Blue dye, which effectively stains proteins within 1 hour and requires only water for destaining. However, sometimes a higher degree of sensitivity is required for in-gel protein detection therefore the silver staining method is chosen. This technique involves the deposition of metallic silver onto the surface of a gel at the locations of the protein bands. Silver ions interact and bind with certain protein functional groups and to attain an effective development of the bound silver to metallic silver resulting in a brown-black color relies upon the use of various sensitizer and enhancer reagents making it a laborious procedure.

This method used for quantification purposes enables the evaluation of purity and yield of the proteins[74]. Absolute quantitation measurements of the amount of Cal B encapsulated in the stomatocytes were attempted using Cal B in its free form as a calibrant.

3.3. Product Quantification Technique

The flow experiments based on the hydrolysis of p-nitrophenyl acetate to p-nitrophenol were conducted to compare the yield of product obtained to compare the reaction performance, when catalyzed by Cal B in its free form and in its encapsulated form and when using nanoreactors with different loading efficiencies as well as to optimize the system in order to achieve maximal productivity. To study these different effects, the product exiting the reactor needed to be quantified for which High Performance Liquid Chromatography was selected.

3.3.1. High Performance Liquid Chromatography

High Performance Liquid Chromatography (HPLC) is an analytical technique used to separate, identify and quantify each compound present in a mixture. This technique relies on pumps to pass a sample mixture known as the mobile phase through a column with

chromatographic packing material (stationary phase) needed to proceed with the separation under high pressures of up to 400 atm. The sample is carried by a moving carrier gas stream of helium or nitrogen. A detector is needed to see the separated compound bands as they elute from the HPLC column. The detector selected is dependent on compound's characteristics. As the mobile phase exits the column, it can either be sent to waste or collected[75]. The components of a HPLC system are presented in Figure 3.7.

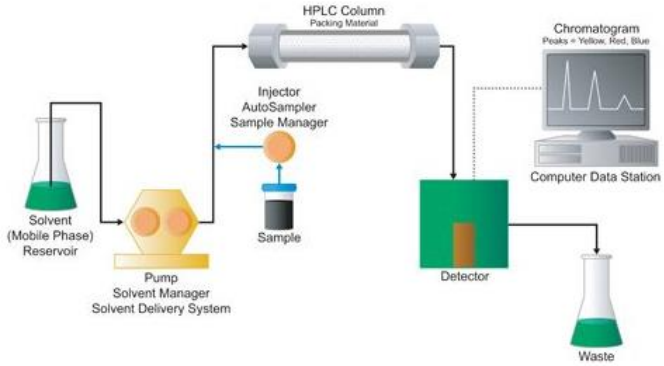

Figure 3.7- High Performance Liquid Chromatography system.

The separation of a sample into its constituents is based on the difference in the relative affinities of the different compounds with the mobile phase and the stationary phase. If a certain compound has a higher affinity with the mobile phase it moves at a faster speed towards the exit of the column and ends up being the first to elute, meaning it has a lower affinity to the stationary phase, while another compound of the same sample mixture with a lower affinity to the mobile phase elutes later[76]. A representation of the separation of components of a mixture is called a chromatogram which displays a series of peaks rising from a baseline as function of time. Each peak represents the detector's response to a different compound in the mixture.

For the quantitative analysis of p-nitrophenol, a calibration curve was traced based on known concentration of the product and their response and therefore the concentration of the product collected at the outlet of the reactor was determined based on the peak areas calculated from the chromatogram.

3.4. Kinetic Model

In recent years, the formulation of mathematical models and the developments of computational tools led to a deeper understanding of chemical reaction kinetics aiding researchers to cope with the overall objectives of improving the safety, yields and quality of the products. Ultimately, a manufacturing process is dependent on its profitability and other economic factors[77].

An insight on the kinetic results is of extreme importance when dealing with catalysts manufacture and comparison. Enzymatic catalysis is of high value in industries too, where normally experiments are carried out with a huge amount of substrate and catalysts and they might show restrictions not considered at the lab scale.

In this context, the importance of modeling arises. The reaction considered in this work does not have relevance in big scale, and the model built does not aim to be comprehensive and detailed, instead it gives an additional tool to this research by allowing us to reproduce our experimental findings and generate new set of results for conditions which we have not tested. The herein discussed model is developed by using experimental kinetic parameters. In this way, the implementation of conditions different from those studied in the lab are also allowed. The model predicts the concentration profiles with time of p-nitrophenol as a result of the hydrolysis of p-nitrophenyl acetate, also taking into account that a small volume of the product formed is due to the self-hydrolysis of the acetate compound in water.

The kinetic is expressed and solved as a set of ODEs (ordinary differential equations), where the concentration is the value varying as a function of the time. The array of time is given as the experimental time (resulted from the Excel grids of the plate reader measurements).

3.4.1. Problem Description

The Cal B catalyzed hydrolysis of p-nitrophenyl acetate follows the well-known Michaelis-Menten law referred to in section 2.3.1.

The experimental procedure behind the determination of the above mentioned parameters is mentioned in section 4.3.1.3 and the subsequent results discussed in section 5.4. The rate of the reaction, even when it does not follow a linear kinetic, it is still namely the variation of the concentration during the reaction time given a certain volume and specifying the initial values of time and concentration.

Knowing this, the ODEs implementation results quite immediately: a set of four ODEs was coded to describe the concentration profiles along the reaction time of the reactant and the product when Cal B was both free in solution and encapsulated. Details on the ODEs are given in the script in the following section.

3.4.2. Mathematical Development

A simple kinetic model is developed in MATLAB®. Two scripts are generated to solve the ODEs set and provide the concentration of reactant and product along the reaction time.

Firstly, a mass balance for the substrate and product are presented in equations (25) and (26), respectively, and were established taking into account the self-hydrolysis of the substrate that occurs in the course of the reaction considered:

$$-\frac{dC_{p-NPA}}{dt} = k_1 \frac{dC_{p-NPA}}{dt} + \frac{C_{p-NPA}(t)V_{max}}{C_{p-NPA}+K_M} \quad (25)$$

$$\frac{dC_{p-NP}}{dt} = k_1 \frac{dC_{p-NPA}}{dt} + \frac{C_{p-NPA}(t)V_{max}}{C_{p-NPA}+K_M} \quad (26)$$

where $C_{p\text{-}NPA}$ is the concentration of p-NPA, $C_{p\text{-}NP}$ is the concentration p-NP, k_1 is the self-hydrolysis constant, V_{max} corresponds to the maximum rate and K_M to the Michaelis-Menten constant. The prediction of the self-hydrolysis constant was difficult, so it could not be included in the model.

The model developed consists of two parts, one being the solver and one containing the set of ODEs needed to be solved. One script (solver) describes the main parameters of the program and it includes the "global" constants used in the calculation (K_m, V_{max} for both Cal B types and initial concentration of reactant and product) and the other contains the set of Ordinary Differential Equations (ODEs) to be solved.

The model considers a set of four ODEs, two for the product formation and the other two for the substrate consumption, including the self-hydrolysis' linear rate mentioned before. The ODEs are expressed as follows:

$$\frac{dC_{substrate}}{dV} = -\frac{V_{max}C_S(t)}{C_S(t)+K_M} \quad (27)$$

$$\frac{dC_{product}}{dV} = \frac{V_{max}C_S(t)}{C_S(t)+K_M} \quad (28)$$

$$\frac{dC_{substrate}}{dV} = -\frac{V_{max_2}C_S(t)}{C_S(t)+K_{M_2}} \quad (29)$$

$$\frac{dC_{product}}{dV} = \frac{V_{max_2}C_S(t)}{C_S(t)+K_{M_2}} \quad (30)$$

where $C_{substrate}$, $C_{product}$, V_{max}, V_{max2}, $C_S(t)$, K_M and K_{M2} denote the substrate concentration, the concentration of product, the maximum rate for free Cal B catalyzed-conversion, the maximum rate for encapsulated Cal B catalyzed-conversion, the concentration of substrate as a function of time, the Michaelis-Menten constant for free Cal B-catalyzed conversion and the Michaelis-Menten constant for encapsulated Cal B-catalyzed conversion, respectively.

3.4.3. MATLAB commands used

The solver is comprehensive for all the constant values (such as initial concentrations and kinetic parameters) and it computes the results via an ODE45 method. Any systems of equations in the form y'=f(t,y) can be solved by all MATLAB® ODE solvers. According to this non-stiff solver, the problem had to be presented in the following way: [t,y] = ode45(odefun,t_{span},y_0), where t_{span} = [t_0, t_f] integrates the system of differential equations y'=f(t,y) from t_0 to t_f with initial conditions y_0. Each row in the solution array y corresponded to a value returned in column vector t. The script is specified in Appendix A. The final curves obtained from the model were plotted together with the experimental data to validate the model which is further discussed in this dissertation.

4. Description of Experiments

4.1. Materials

All chemicals and the enzyme were used as received unless otherwise stated. Ultra pure Milli-Q® water, obtained with the help of a Labconco Water Pro PS purification system (18.2 MΩ), was used for the procedures of polymersomes self-assembly and the rest of the experiments. Dialysis membranes MWCO 12-14000 g mol^{-1} Spectra/Por were used when required. Ultrafree-MC centrifugal filters were purchased from Millipore. Sodium nitrate was purchased from Merck. Candida Antarctica Lipase B (E.C. 3.1.1.3) recombinant from *Aspergillus oryzae* powder 9 U mg^{-1} was purchased from Sigma-Aldrich. 4-Nitrophenyl acetate (E.C. 212-593-5) for synthesis, molar mass 181,15 g/mol, was purchased from Sigma Aldrich. 4-Nitrophenol (E.C. 202-811-7), molar mass 130,11 g/mol, was purchased from Sigma Aldrich.

4.2. Synthetic Methods

4.2.1. Synthesis of Polymersomes

The polymersomes were made using PEG_{44}-PS_{140} copolymers (20 mg), produced by Atom Transfer Radical Polymerization (ATRP) (Appendix B), dissolved in 2 mL of THF and 3 mL of Milli-Q® were added to the solution via a syringe pump at a rate of 1 mL/h, while being stirred at 700 rpm. The final solution was collected into a dialysis membrane 12-14 kDa (Spectrum Labs) and kept under dialysis against Milli-Q® (2 L) for 24 hours, while being stirred at a rate of 560 rpm. The generated polymersome solution was collected from the membrane and stored cupped in the refrigerator at 5-8 ^{o}C.

4.2.2. Stomatocytes Preparation and Encapsulation Procedures

To fold the polymersomes' membrane inward forming a bowl structure (stomatocytes), 300 µL of THF was added to 500 µL of the spherical polymersomes synthesized from PEG_{44}-PS_{140} amphiphilic block copolymers at a rate of 300 µL/h via a syringe pump while mixing the solution at 700 rpm. After an hour, proceeded to do spin filtration for at least 30 minutes using 100 µm centrifugal filters, at a speed of 30000 rpm to remove the organic solvent. The retained fraction was collected from the filters into a vial and added to 1 mL of the biocatalytic aqueous solution (3 mg/mL of Candida Antarctica Lipase B). A second aliquot of THF (150 µL) was added via a syringe pump, after stirring for 30 minutes at 700 rpm, to seal the stomatocytes, promoting their closure to internalize the enzymes within these polymeric structures. It has to be mentioned that the Cal B was especially suitable for the encapsulation, as its contact with organic solvent did not affect at all neither the enzymatic activity nor the intrinsic properties of the catalyst. Nevertheless, via spin filtration again, it was possible to ensure the removal of any enzyme residue from the stomatocyte's surface. Once that all the THF is filtered off and the proper amount of fresh Milli-Q® was replaced in the sample, the final concentration of the sample was adjusted to the initial concentration. The final addition of Milli-Q® water was also necessary to bring the stomatocytes membrane from a flexible form (when the organic solvent

was present) to a rigid form (when only water was the solvent). The biocatalytic stomatocytes were collected and stored cupped in the refrigerator at 5 - 8 ºC.

4.3. Quantification and Activity of the Enzyme

4.3.1 Spectrophotometric Assay

4.3.1.1. Cal B Quantification based on Activity Test

A spectrophotometric assay was conducted based on the test reaction selected for this research, which was the hydrolysis of p-nitrophenyl acetate to p-nitrophenol.

Different volumes of Cal B (2,5 mg/mL) in the required amount of phosphate buffer pH=7,5 were added to p-NPA (5 mM in DMSO, 5,0 µL) to attain the desired enzyme concentration (0, 0,5, 1,0, 1,5, 2, 2,5 and 3 mg/mL) in a total solution volume of 50 µL. A calibration curve was elaborated by monitoring the product formation during 45 minutes at 22 ºC by measuring the increase in absorbance at 405 nm on a Tecan Spark Control V2.1 plate reader and by the formation of a bright yellow compound. Therefore, the product formation was monitored when Cal B stomatocytes and the desired buffer (4:1 v/v) were added to p-NPA (5 mM in DMSO, 5,0 µL) and the response was compared to the response of the known concentrations of Cal B allowing to determine the amount of enzyme encapsulated.

4.3.1.2 Activity of Encapsulated and Non-Encapsulated Cal B

Similarly to the spectrophotometric assay conducted for the quantification of Cal B in stomatocytes the product formation was monitored in the plate reader for 20 minutes at 22 ºC to compare the activity of both enzymatic forms For the free enzyme activity measurement, Cal B (2,5 mg/mL) and phosphate buffer pH=7,5 (4:1 v/v) were added to the substrate p-NPA dissolved in DMSO (5,0 mM, 5,0 µL). As for the measurement of encapsulated Cal B activity, the initial solution was the same as for the free enzyme. The background hydrolysis was measured by the addition of the desired buffer without Cal B to the substrate (9:1 v/v). The resulting slopes of the curves were taken as a measure of the hydrolytic activity. The conversion from relative activity to specific activity (U/mg) was done using the calibration curve of the absorbance of p-nitrophenol.

4.3.1.3 Kinetic Study

The kinetic parameters of both forms of Cal B were estimated to allow a comparison between free and encapsulated systems. The procedure was similar to the one previously described comparing the activity of both forms of Cal B, however to measure the increase in absorbance at 405 nm, different concentrations of substrate were used ranging from 0 to 12 mM. For the kinetic study what matters is the concentration of product formed when using different substrate concentrations. This was calculated by measuring the absorbance of the product (p-NP) which is commercially available at different concentrations and building a calibration curve.

Since the reaction occurs without the presence of Cal B to obtain the true increase in enzymatic reaction rate it was necessary to determine the non-enzymatic reaction rates. When Cal B was present, the enzymatic reaction rate was the sum of both enzymatic and non-enzymatic reaction rates. The true enzymatic rate is obtained by subtracting the non-enzymatic reaction rate. To determine the non-enzymatic rates, the concentration range of p-NPA used was from 0 to 12 mM and phosphate buffer pH=7,5 was added (1:9 v/v). The true enzymatic reaction rates were then plotted against the substrate concentration to produce a Michaelis-Menten model represented by equation (14) in section 2.3.1, for which it was possible to estimate V_{max} and K_M using a second order polynomial fitting of the enzymatic data obtained.

4.3.2. Bradford Assay

Bradford assay was performed for total protein quantitation by using the Coomassie Plus Kit (Thermo Scientific) to confirm the latter. The binding of the Coomassie blue dye to a protein in an acidic medium results in a color change from brown to blue, which changes the maximum absorption from 465 nm to 595 nm. A 2 mg/mL stock solution of Bovine serum albumin (BSA) is prepared and used as a reference. A standard curve of absorbance of solutions versus known concentrations, ranging from 125 to 1500 µg/mL, was made. The stomatocytes samples were previously dissolved in chloroform (4:1 v/v) to ensure that the absorbance measured is not due to the polymeric membrane but only because of the protein. For the test, 30 µL of sample is added to 1,5 mL of Coomasie Plus reagent.

4.4. Analytical Methods

4.4.1. Dynamic Light Scattering

Dynamic Light Scattering analyses were carried out for particle size measurement using the Zetasizer Nano-series instrument (Malvern Instruments, UK). Polymersome, stomatocyte and biocatalytic stomatocyte samples were diluted seven times (100 µL of the sample soluton in 700 µL ultrapure Milli-Q® water) to achieve an acceptable measurement attenuation and polydispersity. The hydrodynamic size of the nanoparticles is given as intensity-average diameter ($z_{average}$) values. Around 150 µL of the diluted samples were placed in disposable micro-cuvettes and used for the analysis. The data was analyzed using Malvern Zetasizer Software 7.12.

4.4.2. Assymetric Flow Field-Flow Fractionation

The asymmetric flow field fractionation-UV-QELS (AF4-UV-QELS) experiments were performed on a Wyatt Eclipse AF4 instrument connected to a Shimadzu LC-20A Prominence HPLC system equipped with a Shimadzu CTO20A column oven. The AF4 was further connected to the following detectors: a Shimadzu SPD20A UV detector, a Wyatt DAWN HELEOS II light scattering detector (MALS) installed at different angles (12,9º, 20,6º, 29,6º, 37,4º, 44,8º, 53,0º, 61,1º, 70,1º, 80,1º, 90,0º, 99,9º,109,9º, 120,1º, 130,5º, 149,1º, and 157,8º) using a laser operating at 208 nm, a Wyatt Optilab Rex refractive index detector and a QELS

detector installed at an angle of 140,1º. Detectors were normalized using Bovine serum Albumin (BSA). The AF4 channel was pre-washed with running solution of 1,5 mM $NaNO_3$, which was also used for the separation. The processing and analysis of the data was performed using Astra 6.1.1.AII. AF4 separations were performed on an AF4 short channel with regenerated cellulose (RC) 10 kDa membrane (Millipore) and spacer of 350 µm.

4.4.3. SDS-PAGE

SDS-polyacrylamide gel electrophoresis was performed using a Miniprotean tetra-cell (Bio-Rad), 4-20% running gel. To estimate the Cal B enzyme's yield (quantity) in the stomatocytes, a calibration curve was designed by running a dilution series of free enzyme and two samples of stomatocytes filled with the same enzyme in parallel, as well as Dual Color protein standard (Bio-Rad) was electrophoresed on the SDS-PAGE gel. The Dual Color protein standard (Bio-Rad) was used since its MW range is from 10 to 250 kD and the enzyme under analysis has an expected MW of 33 kDa. The effective dilution series had a dilution factor of 2 obtaining 3 ppm, 1,5 ppm, 0,75 ppm and 2 ppm, 1 ppm and 0,5 ppm of free enzyme solution, of which 40 µL was mixed with 10 µL of 4X loading dye. As for the samples of stomatocytes filled with enzyme, 40 µL were collected and heated at 90 ^oC during 3 to 5 minutes to degrade the polymeric structure and mixed with 10 µL of 4X loading dye. The gel was processed with the Pierce Silver Stain Kit (Thermo Fischer Scientific) for an effective staining, followed by destaining to visualize the protein bands. Coomassie Blue did not prove effective for staining since this protein required a higher sensitivity. The destained electrophoresis gel was captured using IQuant Capture 350 GE. However, this method did not serve the purpose of quantifying the amount of Cal B encapsulated within the nanoreactor. In fact, while the Coomassie was not sensitive enough to visualize the protein, the silver agent turned out to be too sensitive, resulting in several bands that made the analysis of the intensity difficult. On the other hand, this method proved the effective internalization of the enzyme.

4.4.4. High Performance Liquid Chromatography

The product collected at the outlet of the reactor was separated from the catalytic stomatocytes and quantified using HPLC.

The column used for the analysis was GraceSmart RP 18 5u column (150 mm × 4.6 mm) and water with 60% of ACN was used as eluent. The total run time was 8 minutes and the peak corresponding to the product formed is identified at 2 to 3 minutes from the start of the run. For the quantitative analysis of the product formed, peak areas were used, and a calibration curve was constructed. This calibration was based on different injection volumes using an autosampler starting from a 0,01 mg/mL of p-NP solution. This method improves the precision and accuracy of results, where volume errors are difficult to predict and control. A standard curve was elaborated by plotting the concentration of p-NP and corresponding responses. Therefore, the response of the product collected at the outlet of the reactor was compared to the response of the known concentrations, which allowed to determine the amount of p-nitrophenol formed. To identify the peak that corresponds to the product, the retention factor

and response of the peak in the chromatogram of the standard solution (p-nitrophenol) were compared with the sample chromatogram.

4.5. Imaging Techniques and Analysis

4.5.1. Scanning Electron Microscopy

Polymersome, stomatocytes as well as biocatalytic stomatocytes samples were diluted seven times with ultrapure Milli-Q® water to obtain a clearer visualization of the nanoparticles' morphology through SEM. 5 µL of the diluted solution is placed on a silicon wafer that was washed in 70% EtOH and dried for 24 h. All the samples drop casted on the silicon wafer were gold sputtered prior measurements for 30 seconds at 60 mA, the sputtering procedure allowing the deposition of a thin layer of metal on the sample surface (ca. 3 nm), which is made visible in the microscopy.

All SEM analyses were operated at 10KV with a spot aperture of 4.5 in a SEM-FEI-FIB.

4.5.2. Transmission Electron Microscopy

TEM images were recorded by a FEI Tecnai 20 (type Sphera) at 200 kV. 10 µL of sample was dropped onto a carbon-coated copper grid. After removing the solution by blotting paper, the samples were dried at ambient conditions. For staining, a drop of phosphotungstic acid (2%) solution was placed on the grid for 30 s.

4.6. Flow Experiments

4.6.1. Continuous flow reactor system – hydrolysis of p-NPA to p-NP

The performance of stomatocytes filled with Cal B was evaluated in comparison to the performance of free enzyme (Cal B) when catalyzing the hydrolysis of p-NPA to p-NP in a continuous flow setup.

For the flow experiments, two different setups were used which consisted of cylindrical tubes mimicking plug flow reactors. Both the systems had the same effective length of 20 cm, but different internal diameters (ID). The smaller setup had an internal diameter of 3,1 mm, while the bigger setup had an internal diameter equal to 4,1 mm.

For the flow experiments, prior to the substrate (5 mM p-NPA dissolved in DMSO) being fed at the inlet of the reactor (2,5 mL for bigger flow setup and 1,5 mL for smaller flow setup) via a syringe pump at a rate of 0,5 mL/h, the catalyst and phosphate buffer pH=7,5 solution (1:2 v/v, total volume of 1,8 mL for bigger flow setup and 1,6 mL for smaller flow setup) were inserted at the inlet of the reactor. To test the performance of the reaction when catalyzed by the free enzyme, a 2,5 mg/mL Cal B solution was used. Eventually, the product along with the catalyst was collected at the outlet of the reactor.

The reaction in both setups was conducted under the same conditions and in the same manner. The flow experiments were performed to study the effect of encapsulated Cal B, the

effect of Cal B load in the nanoreactors and even the effect of space-time on the product outcome as an attempt to optimize the system.

4.6.2. Leaching and reusability of the biocatalytic stomatocytes

The product and catalyst were collected at the outlet of the reactor, as it was stated previously. The sample collected at the outlet of the reactor was placed in 100 nm centrifugal filter units (Merck) to recover the nanoreactors through centrifugation. The stomatocytes were recovered through spin filtration using the centrifuge MSE Mistral 1000, washed with Milli-Q® and ready to be reused. The leaching was an important factor to prove that the activity loss of the encapsulated Cal B was not due to the flow configuration. To estimate the leaching, the fresh sample of stomatocytes and the sample recollected after 5 cycles of reuse were measured in terms of their specific activity via the spectrophotometric assay and the amount of Cal B left in them via the Bradford assay.

5. Results and Discussion

5.1. Shape and Morphology Characterization

Stomatocytes are prepared by inducing a shape transformation in the polymersomes creating a cavity to facilitate the confinement of biocatalysts. To validate the encapsulation procedure, various techniques were used to demonstrate whether the entrapment of Cal B was successful. Firstly, it was important to verify if the morphology and size acquired by these nanostructures is adequate. The polymersomes self-assembled from PEG_{44}-PS_{140} copolymers were formed and they appeared to have a uniform spherical shape (Figure 5.1A), in Figure 5.1B the open stomatocytes are shown, result of the first addition of THF and Figure 5.1C confirmed the closure of the rigid stomatocytes' neck after the encapsulation of Cal B. The formation of polymeric vesicles was expected since the hydrophilic block (PEG) covers 24% of the amphiphilic block copolymer used for the synthesis of polymersomes, keeping in mind that it is required to be at least around 25% to acquire this morphology[32].

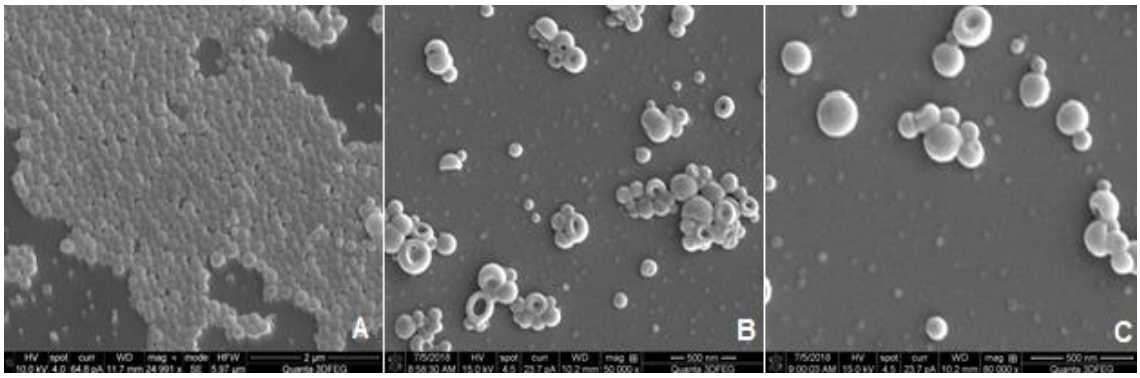

Figure 5.1- Stomatocytes formation via the solvent addition method. (A) SEM of polymersomes at the beginning of the shape transformation (2 μm scale bar); (B) SEM of the open neck stomatocytes following the first addition of THF (500 nm scale bar); (C) SEM of the closed stomatocytes containing Cal B following the addition of a second aliquot of THF (500 nm scale bar).

In terms of size, DLS measurements were made to check the dimension of these nanostructures.

The nanosystems attained an average diameter between 150 and 165 nm (Figure 5.2). A slight increase in diameter was verified in the catalytic stomatocytes, which was expected after encapsulation. The intensity of the fluctuations visualized was characteristic of a dispersion of small particles as seen in Figure 9.1 of Appendix C. The PdI was very low (<0,2) meaning that the nanoparticles did not tend to aggregate, and a high degree of order is attained.

The correlogram of the polymersomes (Figure 9.2 in Appendix C) and the catalytic stomatocytes (Figure 9.3 Appendix C) shows that the correlation of the signal does not take a long time to decay, which also supports the low polydispersity of the samples[64]. A polydispersity of morphology is not seen from the SEM and DLS measurements since there is no variety in shape, ensuring that it is not necessary to resort to filtration or size exclusion

methods. However, further characterization techniques were used to ensure that the enzyme is effectively internalized within the stomatocytes.

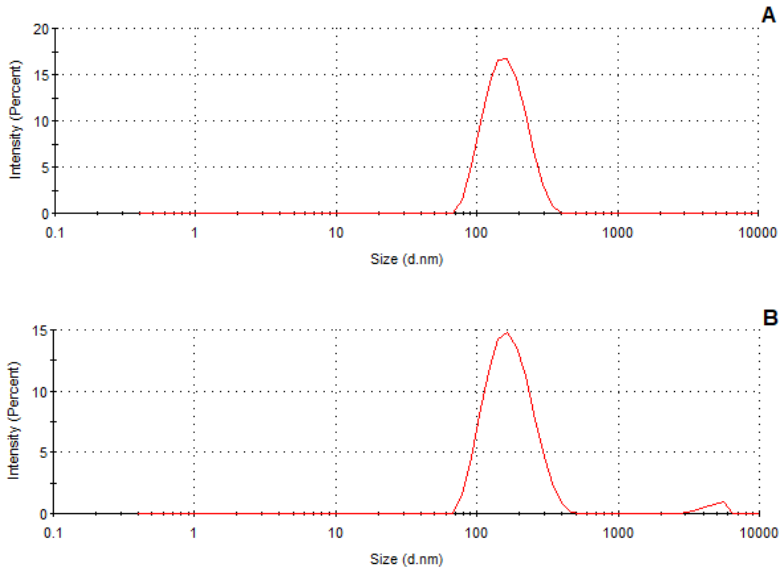

Figure 5.2- DLS measurements. (A) Size distribution of polymersomes; (B) Size distribution of stomatocytes.

As for the AF4 measurements, the separation relies on the difference between the diffusion coefficients of the particles with the smallest particles eluting first. For the analysis, aliquots of Cal B and their mixture with empty stomatocytes were injected in the AF4 separation channel. Cal B enzyme was the first to elute within the first minutes and the stomatocytes much later due to their larger size and therefore smaller diffusion coefficient (Figure 5.3A). Stomatocytes filled with Cal B showed only one peak corresponding to the filled stomatocytes and the peak which corresponds to the pure enzyme isn't noticeable at low retention times. This

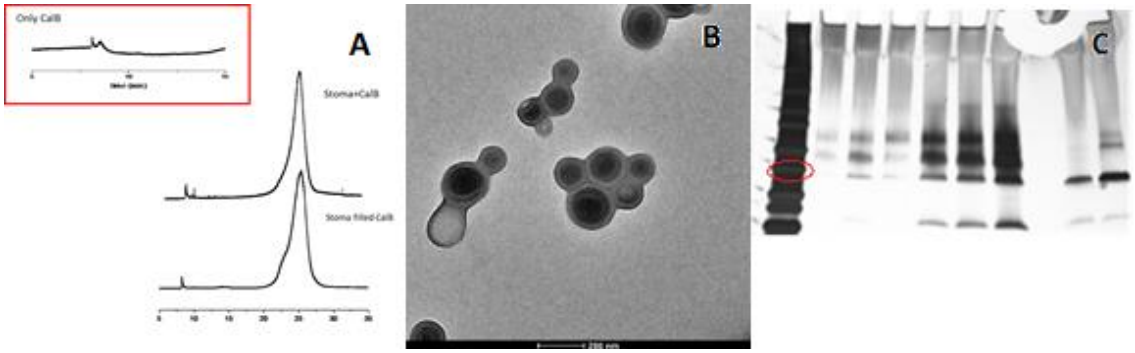

Figure 5.3- Characterization techniques to prove the successful encapsulation of Cal B. (A) Asymmetric field flow fractionation for the stomatocytes filled with Cal B and their comparative elution to the controls: empty stomatocytes and pure enzymes; (B) Transmission Electron Microscopy of the stomatocytes filled with enzyme; (C) SDS-page analysis of the stomatocytes filled with Cal B using different concentrations of Cal B as standards as means of comparison (red circle indicating the band corresponding to the enzyme's MW).

indicates that the enzyme is well confined within the stomatocytes and is not adsorbed on their surface. The elution time for Cal B filled stomatocytes appears to be the same as for the empty stomatocytes meaning that the stomatocyte's size is maintained prior to the encapsulation procedure. The enzyme's internalization was also proved by TEM (Figure 5.3B) showing completely closed stomatocytes and the strong contrast visible indicates that Cal B is well confined inside them. Although these techniques are reliable, the presence of the enzyme in the nanostructures was also confirmed by SDS-page analysis (Figure 5.3C).

5.2. Quantity of Cal B Loaded into Stomatocytes: Loading Efficiency

A calibration curve was elaborated via a spectrophotometric assay correlating the absorbance per minute with the concentration of Cal B standard solutions. This correlation is viable due to the Beer-Lambert law where the absorbance is directly proportional to the enzyme concentration in the sample used for the assay as given in equation (24). The slopes of the curves obtained for each standard solution were taken as a measure of the hydrolytic activity and the measured slope of background hydrolysis of p-NPA to p-nitrophenol was subtracted from the Cal B-catalyzed conversion and multiplied by a factor of 60, to convert the units into minutes instead of seconds. The standard curve in Figure 9.4 section D1 of Appendix D was built to determine the encapsulation efficiencies, knowing that a 3 mg/mL of Cal B solution was used when preparing the catalytic stomatocytes. In general, the results of the loading efficiency obtained from the spectrophotometric assay were an overestimation when compared to the values obtained from the Bradford assay which is a more accurate method for protein quantification. The Bradford assay calibration curve obtained using BSA as a reference protein is presented in Figure 9.5 using the data displayed in Table 9.2 (Appendix D section D2).

Based on the standard curve equation, the loading efficiencies of the various Cal B stomatocytes samples were calculated using the values of absorbance at 595 nm measured for six samples (Table 9.2 Appendix D section D2). Based on these values made for each sample, the average encapsulation efficiencies were determined, but were not consistent (Figure 5.4). This variation can be due to the purification method not being the same for all the samples prepared (e.g. spin filtration time, speed, different washing volumes, use of different centrifugal units). The error bar for each sample's loading efficiency was obtained based on two samples both prepared on the same day and under the same conditions which lead to similar loading efficiency values.

However, the inconsistency of the loading efficiencies made the catalyst load a considerable variable when testing the nanoreactors' performance in flow and its effect is further discussed in section 5.5.2.

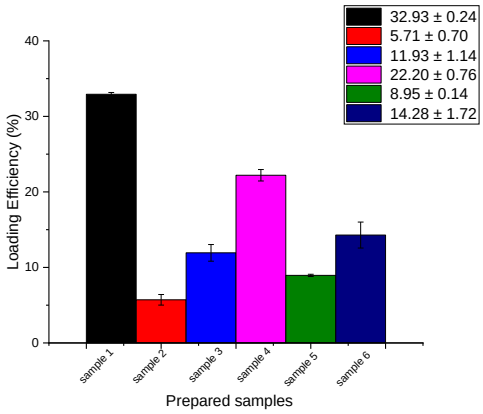

Figure 5.4- Loading efficiencies for different stomatocytes filled with Cal B samples.

5.3. Activity of Encapsulated Cal B and Non-Encapsulated Cal B

The results obtained from the Bradford assay were useful to calculate the specific activity (U/mg) of the stomatocytes filled with Cal B and compare them to the specific activity of the free enzyme.

The activity tests performed were helpful to determine the specific activity of Cal B in both its forms. The specific activity was calculated using the following expressions,

$$\Delta Abs = (\Delta Abs_{Cal\ B} - \Delta Abs_{BG}) \times 60 \quad (31)$$

$$U_{total} = \frac{\Delta Abs}{slope\ calibration\ curve} \quad (32)$$

$$Activity\ (U/mg) = \frac{U_{total}}{amount\ of\ Cal\ B\ (mg)} \quad (33)$$

where $\Delta Abs_{Cal\ B} - \Delta Abs_{BG}$ is the difference between the slopes given by the increase in absorbance when the test reaction was catalyzed by Cal B and the background absorbance (substrate+buffer) and U_{total} is the total activity of the enzyme. The calibration curve slope corresponds to the Cal B calibration curve obtained from the spectrophotometric assay mentioned in section 5.2. The specific activity was calculated based on the equations above for samples with a high amount of Cal B as well as for a low amount of Cal B. The ratio of the specific activity relative to the free enzyme's activity was reported (Table 5.1). The specific activity of the free enzyme was 21,5 ± 2,8 U/mg calculated based on the values obtained from two assays given in Table 9.3 Appendix E. As it was mentioned before the amount of Cal B in the stomatocytes can be a good indication of the extent of its influence on the activity.

Table 5.1- Enzymatic activity after encapsulation compared with that of the free enzyme.

	Sample 1	**Sample 2**
Loading efficiency (%)	33,8	6,3
Ratio of specific activity relative to free enzyme activity	8,2	1,2

We report that the enzyme was more active when entrapped. Stomatocytes which have a high loading efficiency are expected to have a high specific activity.

5.4. Kinetic Parameters of Encapsulated Cal B and Non-Encapsulated Cal B

It is particularly important to know the intrinsic kinetic properties of encapsulated Cal B in comparison to its free form, offering an insight on its capability of being employed in a bigger scale process.

In order to obtain the enzymatic rate of Cal B in mM/min as a function of substrate concentration, the increase in absorbance at 405 nm needed to be obtained from the spectrophotometric assay, when monitoring both forms of Cal B-catalyzed conversion (Figure 9.6 and 9.7 of Appendix F) and non-enzymatic conversion (Figure 9.8 Appendix F) as well, using different concentrations of para-nitrophenyl acetate. This data had to be converted into the increase in product observed as the reaction takes place. A calibration curve correlating the increase in absorbance at 405 nm with the concentration of p-nitrophenol standard solutions (Figure 9.9 in Appendix F) was used to obtain the product formation as a function of time, for the reaction catalyzed by free enzyme and by encapsulated enzyme displayed in Figures 5.5 and 5.6, respectively, as well as the non-enzymatic product formation (Figure 5.7). The slopes of these curves were taken as a measure of the product formation rate, thus obtaining the true enzymatic rate by subtracting the non-catalyzed conversion rate from Cal B-catalyzed conversion rate. Therefore, by plotting the true enzymatic rates against the substrate concentration range (Table 9.4 and 9.5 in Appendix F) saturation curves following the Michaelis-

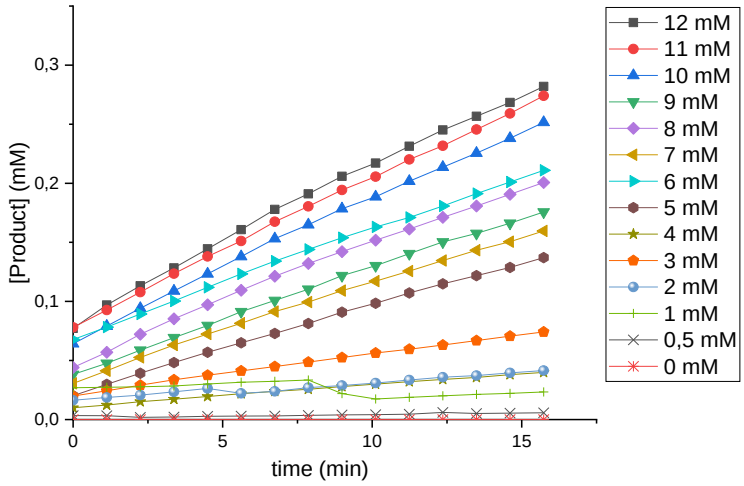

Figure 5.5- Product formation as a result of free Cal B catalyzed conversion of p-NPA to p-NP.

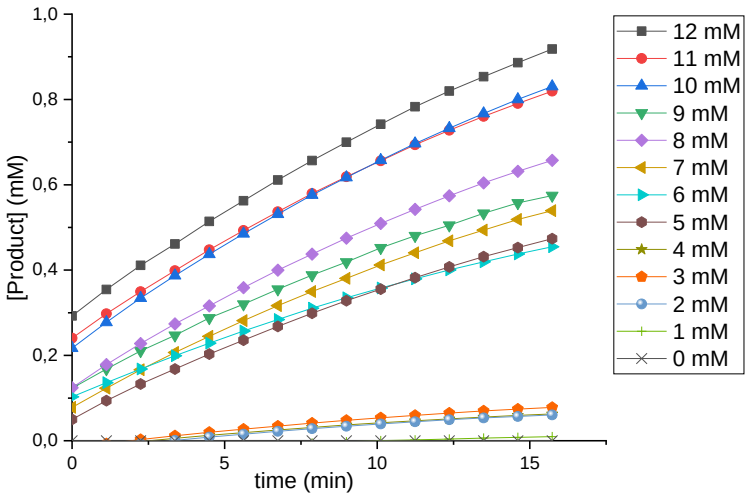

Figure 5.6- Product formation as a result of encapsulated Cal B catalyzed conversion of p-NPA to p-NP.

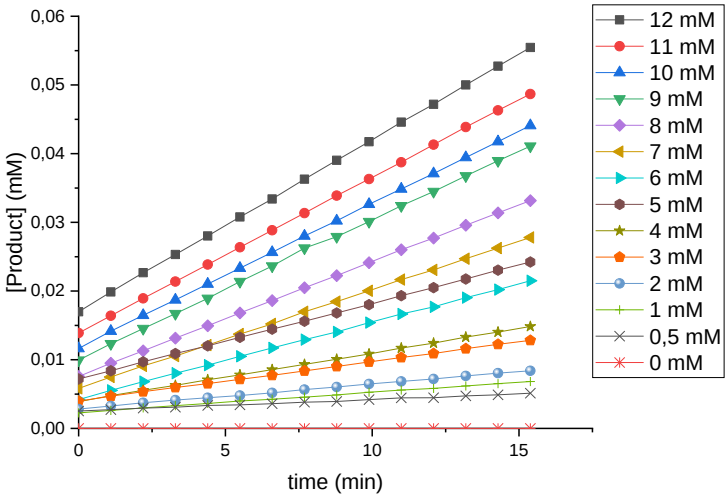

Figure 5.7- Product formation as a result of non-catalyzed conversion of p-NPA to p-NP.

Menten model were obtained (Figure 5.8), for which it was possible to estimate V_{max} and K_m that were further used as comparative parameters to study the kinetics behind both forms of Cal B. The kinetic parameter V_{max} was used to estimate the turnover number, k_{cat}, for both forms of Cal B since it was considered a valuable parameter for bigger scale applications. A fair comparison between the encapsulated and non-encapsulated form of Cal B in terms of their kinetic properties was made.

Some points from Tables 9.4 and 9.5 (Appendix F) were discarded when trying to obtain a better second order polynomial fitting of the enzymatic data obtained.

The maximum rate, V_{max}, is defined as the rate achieved when the enzyme molecules are saturated by substrate molecules, while the Michaelis-Menten constant, K_m, corresponds to the substrate concentration when the reaction rate is brought down to half of its maximum value. The equations of the saturation curves (Figure 9.10 and 9.11 Appendix F) are needed for the calculation of K_m and, by equalizing them to $V_{max}/2$, the desired value is determined. The value for V_{max} is equal to the rate attained when high substrate concentrations are used, in this

case 12 mM, or when the saturation curves reach equilibrium. The variations observed in these parameters when the test reaction is catalyzed by either encapsulated Cal B or by free enzyme powder are displayed in Table 5.2.

As reported in Table 5.2, V_{max} value of encapsulated enzyme resulted to be higher than the value achieved for free enzyme. Since V_{max} can be considered an indication of efficiency of a reaction this means that a reaction catalyzed by Cal B in its encapsulated form attains higher reaction rates, making the hydrolysis of p-NPA to p-NP more efficient when catalyzed by entrapped Cal B than by free Cal B. This aspect reflected on the value of k_{cat}, which was higher once again for entrapped Cal B than for the free enzyme.

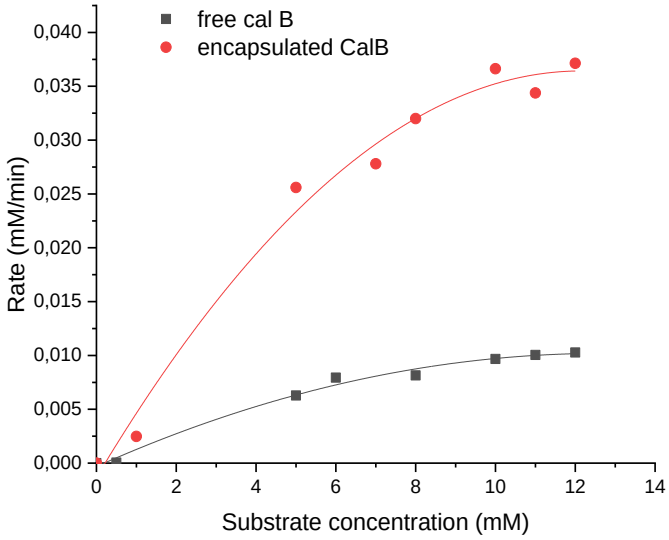

Figure 5.8- Polynomial Fitting of Michaelis-Menten model of enzymatic rate data for Cal B in its free form and in its encapsulated form.

Table 5.2- Kinetic data for non-encapsulated and encapsulated Cal B.

	Free Cal B	**Encapsulated Cal B**
V_{max} (mM h^{-1})	0,62	2,23
k_{cat} (s^{-1})	157,0	945,6
K_m (μM)	3790,1	3906,5

On the other hand, the K_M values which are related to the affinity between substrate and enzyme molecules were similar for Cal B in its encapsulated form and in its free form, suggesting that the affinity of the stomatocytes filled with Cal B towards the substrate was not so different from the free Cal B. This also proved that encapsulation of the enzyme does not affect its intrinsic properties.

5.5. Enzyme Performance in Flow: Effects of Encapsulation, Catalyst Load and Space-Time

Considering the high turnover number observed for encapsulated Cal B, activity in a continuous flow fashion was also evaluated. The performances of free Cal B and encapsulated Cal B with different loading efficiencies were tested by carrying out the same reaction in two continuous flow systems.

As mentioned before, high performance liquid chromatography was used to determine the concentration of the product in the sample collected at the outlet of the reactor. A calibration curve to determine the amount of product formed when evaluating the effects of encapsulation, catalyst load and space time is shown in Figure 9.12 in Appendix G. It is important to point out that the activity achieved in flow was expressed in terms of yields of p-nitrophenol formed.

5.5.1. Effects of Encapsulation

It was decided to study the effects of encapsulation in both the milli-flow systems. The peak areas are obtained from the chromatogram, as the example given in Figure 9.13 in Appendix G shows that the product elutes 2 to 3 min after the start of the separation. The yield of product, $Y_{p\text{-}NP}$, was calculated based on equation (34), knowing that p-nitrophenol is not injected at the inlet of the reactor ($n_{p\text{-}NP}$ (in)=0), the results being given in Table 9.6 in Appendix G.

$$Y_{p-NP}(\%) = \frac{n_{p-NP}(out) - n_{p-NP}(in)}{n_{p-NPA}(in)} \quad (34)$$

For the free and encapsulated enzymatic systems, it was clearly visible that the encapsulation of Cal B had a pronounced effect on the yield of product, when employed in the smaller flow system (Figure 5.9B), as compared to the bigger flow system (Figure 5.9A). This result suggested that mass transfer was hindered due to the presence of a high amount of catalyst in solution, when using free enzyme[78] (2,5 mg/mL), hampering the substrate from reaching the enzyme's active sites[18][79]. The activity observed for the stomatocytes' sample also looked quite low. However, in the first test, the amount of enzyme confined in the stomatocytes was lower (6,3%), so it can be concluded that overall the reaction did not suffer from significant mass transfer limitations and the low yield only depended on the small amount of catalytic material employed. When the reaction was performed in the small flow-reactor, an improved yield of product was obtained for both the cases. In this case, the better performance of the nanoreactors was clearer, and it can be attributed to its high surface to volume ratio, having a good dispersion in solution thereby enhancing the diffusion of the substrate as well as improving the activity[36]. Obviously, the enhancement in the overall process was strongly dictated by the use of a smaller reactor volume which favored the contact between catalyst and substrate.

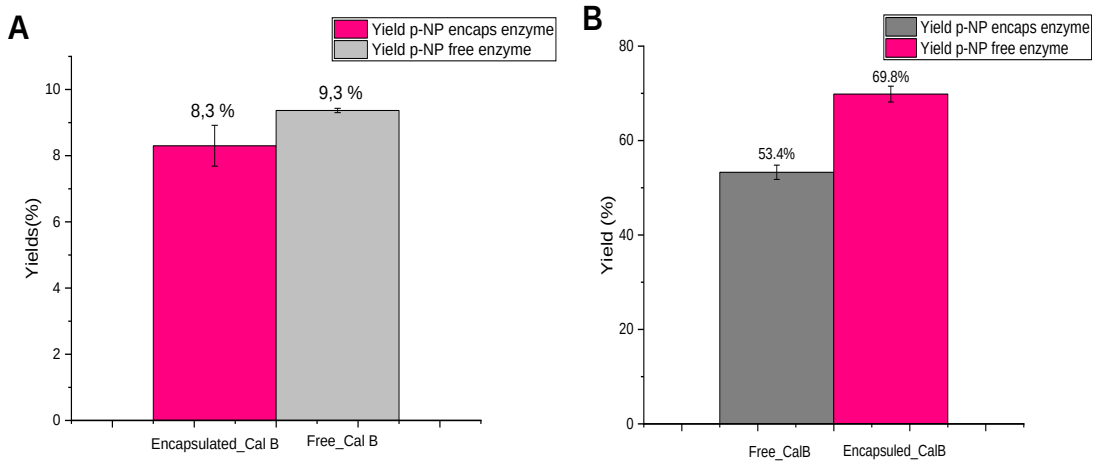

Figure 5.9- Yields of products attained in the two continuous flow setup using free enzyme or encapsulated enzyme. (A) Bigger flow setup (ID=4 mm); (B) Smaller flow setup (ID= 3,1 mm).

5.5.2. Effects of Catalyst Load in the Nanoreactors

The nanoreactors' stability was tested by performing leaching experiments in the bigger setup employing samples with different loading efficiencies in flow. These experiments were conducted to verify whether this phenomenon was dependent on the amount of catalyst confined within the nanoreactor and to explore the extent of the nanoreactors' reusability. However, leaching was expected since these nanoreactors were non-crosslinked systems as verified in previous works[80]. The interaction of the catalyst with DMSO used to solubilize the substrate as well as the flow system's hydrodynamics also contribute for the loss of catalyst confined within the nanoreactors. The results of the leaching experiments were expressed in terms of activity loss relative to the fresh sample's activity. The relative activity following each cycle of reuse is shown in Table 9.7 in Appendix G.

Figure 5.10 shows that a higher loaded nanoreactor (33% loading efficiency) experienced a great loss in activity after the first cycle of reuse, reaching a very high value that remained approximately stable for the following cycles of reuse. Meanwhile, when a lower amount of Cal B was present in the stomatocytes (6% loding efficiency), it did not suffer a great loss in activity during the first cycle and the same tendency to stabilize on a certain value was observed as for the higher loaded nanoreactor during the following cycles. Besides this, in the latter case, the yield of product achieved was very low making it impractical for any type of application. Using an intermediate loaded sample (14% loading efficiency) led to better results in general, its activity loss stabilizing at a more reasonable value (<50%) after the second reuse cycle. The encapsulated enzyme also retained its activity during the first cycle (~98%) suggesting that this intermediate value could be more suitable for bigger scale processes.

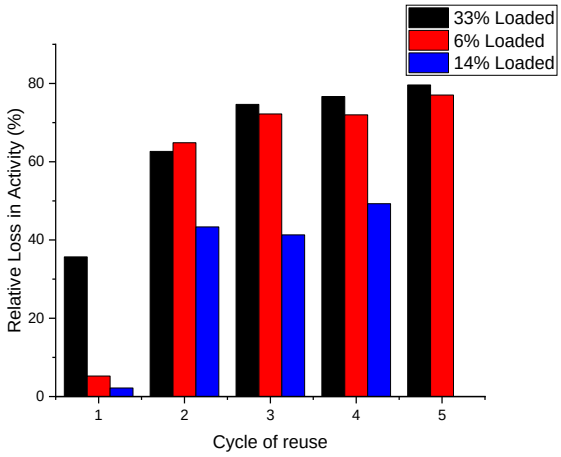

Figure 5.10- Losses in activity relative to the fresh sample's activity during the reusability process (5 cycles of reuse).

In order to probe whether the activity loss was caused by enzyme deactivation or by leaching, the enzyme activity as well as the loading efficiencies were measured at the end of the 5 cycles of reuse and compared to their initial values (Table 5.3).

Table 5.3- Loading efficiency and specific activity obtained for the fresh stomatocytes and after leaching experiments for the samples tested.

Experiments		Initial	After 5 cycles
1	Loading efficiency (%)	33,8	11,1
	Specific activity (U/mg)	160,3	15,1
2	Loading efficiency (%)	6,3	2,3
	Specific activity (U/mg)	23,4	11,8

The results confirmed that the drop in activity during the cycles of reuse were due to leaching, which was verified based on the values from Table 5.4. This also can be explained by the stomatocytes losing enzyme during centrifugation and transfer affecting the total recovery, although this is not expected to have a big influence on the results considering the very narrow size of the filters. For the higher loaded stomatocytes the percentage of leaching (~70%) was close to the activity loss percentage achieved in the flow experiments. The leaching was improved when a lower loaded sample of stomatocytes was employed in flow.

Table 5.4- Leaching obtained for the higher loaded sample and for the lower loaded sample.

Initial	After 5 cycles	Relative loss of Cal B (%)	Leaching (%)
33,8% load	11,1% load	32,9	67,1
6,3% load	2,5% load	39,7	60,3

5.5.3. Effects of Space-Time

To investigate the influence of space time on the overall performance of the reaction catalyzed by the nanoreactors, the productivity in the two setups was calculated using equation (35) and presented in Figure 5.11.

$$Productivity\ (p-NP) = \frac{n_{p-NP}(out)}{V_{reactor} \times \tau} \qquad (35)$$

where n_{p-NP}, n_{p-NPA}, $V_{reactor}$, τ denote the number of moles of product formed, the number of moles of substrate that enter the reactor, the volume of the reactor and the space time of the reactor, respectively. The values for each parameter considered for calculating the productivity are summarized in Table 5.5.

Table 5.5- Productivity attained by varying the space-time and using nanoreactors with different Cal B load.

Nanoreactor load	$n_{p\text{-}NP}$ (out) (mmol)	$V_{reactor}$ (mL)	τ (min)	Productivity (μmol $mL^{-1}min^{-1}$)
8%	1,39E-03	1,5	3	155,2
33%	4,68E-03	2,5	5	16,5
6%	2,12E-03	2,5	5	7,53
14%	9,37E-03	2,5	5	33,3

The productivity achieved in the smaller setup is much higher even though a lower loaded stomatocytes sample (8% loading efficiency) was used, which highlights that homogeneity of the reaction mixture was an essential factor to improve the overall performance of a reaction, since it promotes a better contact between the enzyme and substrate molecules, leading to a better product outcome. Similarly, to what was observed in the experiments using free enzyme, a decrease in productivity was observed when stomatocytes with higher loading efficiency are applied[45]. This effect was caused by diffusional limitations occurring throughout the system, inhibiting mass transfer; the presence of a higher amount of Cal B in the stomatocytes in the process made it more difficult for the substrate to penetrate further into the particle, hindering it from reaching the enzyme's active sites.

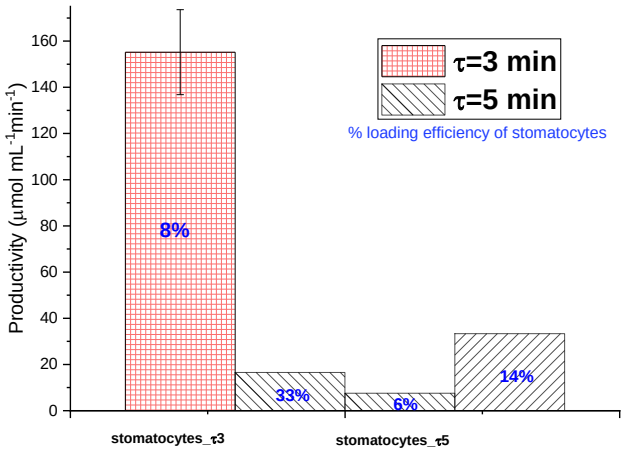

Figure 5.11- Productivity achieved in the two setups by using stomatocytes with different load of Cal B.

5.5.4. Improvement of the Process

The studied effects are crucial for improving the system's efficiency as to obtaining a better productivity and contributing to the development of an optimal system. Following this research, it was found that conducting a reaction in a smaller reactor combined with the use of nanoreactors with a lower load of catalyst can lead to an improved reaction performance. The selection of a smaller sized milli-flow reactor was seen as the better alternative, since it promotes a higher degree of contact between the catalyst and substrate, which is dependent on micromixing and dispersion. Previous work in process research and development[60] suggests that the micromixing time is reduced as an increase in Reynolds number, Re, is verified, as a consequence of an increase in linear flow rate. The tests in both reactor setups were conducted under the same reaction conditions (i.e. equal flow rate), so the linear velocity of the reaction mixture can be used as a comparative parameter since the size of the reactor varies. The flow rate, Q, is given by:

$$Q = u \times A_{reactor} \quad (36)$$

being u the linear flow velocity and $A_{reactor}$ the area of the tubular reactor's cross section. This fact can possibly explain the improved results obtained when a tubular reactor with an ID of 3,1 mm is used since the linear velocity inside the reactor is higher than in the reactor with an ID of 4,1 mm (Table 5.6).

Table 5.6- Linear flow velocity inside both reactor setups.

Reactor ID (mm)	A (mm^2)	v (cm/min)
3,10	7,50	6,67
4,10	12,5	4,00

Based on the kinetics of the test reaction and observing the product formation of the test reaction, it can be classified as a fast reaction with reaction time below 10 minutes (type B) being kinetically controlled in reactors with high micromixing efficiencies. A Damkőhler number, Da, below 0,001 defines maximum mixing time limits beneficial for type B reactions. Since the space time of the smaller milli-flow reactor was 3 minutes, and of the bigger milli-flow reactor 5 minutes, the test reaction requires a maximum mixing time of 0,18 s and 0,3 s, respectively. Tube reactors need a certain minimum flow rate to obtain good mixing and the introduction of a static mixer could possibly improve this aspect in the bigger milli-flow reactor, which could play an important role when scaling up a process.

According to Gobert et al.[60], the dispersion increases as the diameter of a reactor increases thereby deviating from plug flow. So, in this case, it can be assumed that the smaller milli-flow reactor provides lower dispersion (low Bo) and higher diffusion, which can explain the better product outcome verified.

As for the catalyst load within the nanoreactor, it was preferable to use stomatocytes with a lower loading efficiency because it would not impose mass transfer limitations, therefore facilitating the contact between the catalyst and the substrate to occur smoothly. Beside this,

the extent of leaching is not significant as compared to when a higher loaded nanoreactor is employed.

The various effects on the product outcome, encountered when employing the nanoreactors in flow, and seeking approaches to optimize the process, emphasized its potential for larger scale processes. Additionally, a mathematical model was generated to simulate the performance of the reaction considered.

5.6. Kinetic Model

The model is based on the practical assumption that in the spectrophotometric assay conditions, no mass transfer limitations occur. This was a reasonable assumption because of the small volume of substrate used and the low enzymatic concentration. The developed model does not consider the amount of catalyst used, but the experimental parameters previously found for those specific set of experiments and displayed in Table 5.2. Therefore, the model can only be used to determine the amount of product formed when varying the initial concentration and when extending the reaction time (t,y output).

The self-hydrolysis constant was difficult to predict so it was not included in the model. Therefore, the absorbance resultant from the self-hydrolysis (background) was subtracted from the absorbance resultant from the product formation.

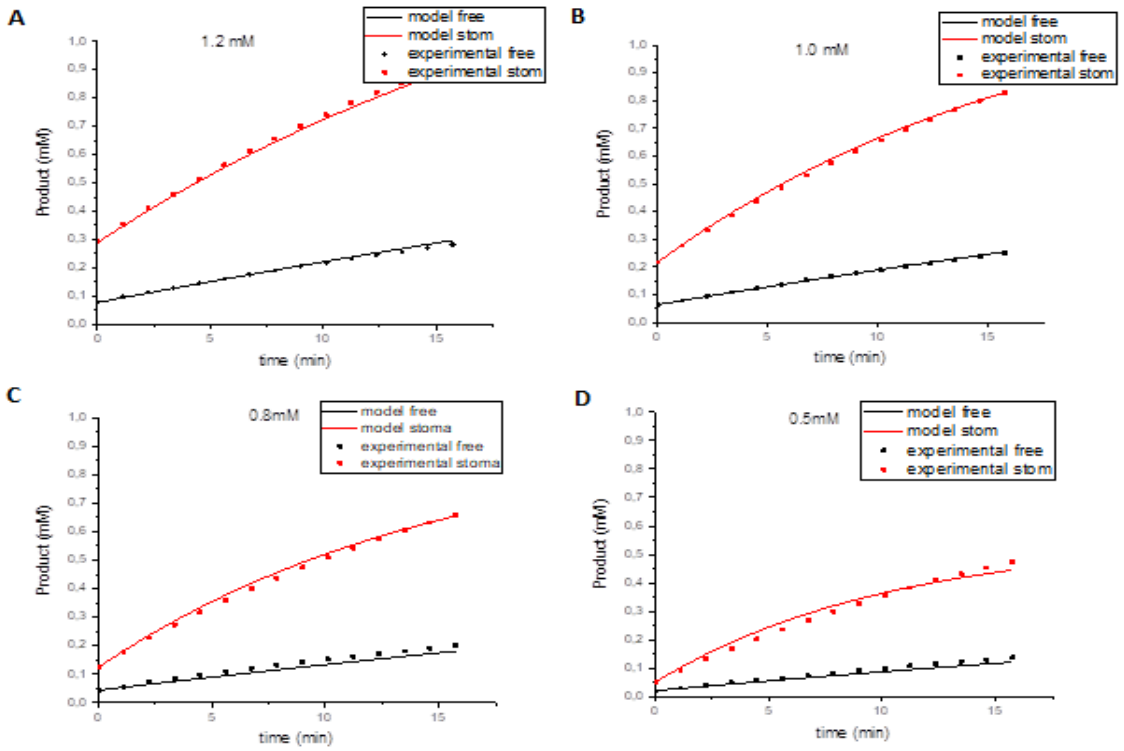

Figure 5.12- Experimental data (dots) collected and model predictions (lines) for the reaction rate of the p-NPA hydrolysis when the experiments were performed at different concentrations of substrate in solution (p-NPA). (A) [p-NPA] = 1,2 mM; (B) [p-NPA] = 1,0 mM; (C) [p-NPA] = 0,8 mM; (D) [p-NPA] = 0,5 mM.

The results shown in Figure 5.12 show a good agreement between the model and the experimental data obtained, when guess values for the kinetic constant of the self- hydrolysis of p-NPA (k) are given in the script. Also, it can be seen that the model had a better fitting with the experimental data for the test done using higher substrate concentrations, verified in Figures 5.12A and 5.12B. In fact, when the concentration of substrate was lower the value of k should decrease, but this decrease was not as linear as for the other concentrations and more difficult to predict.

Overall, the model and the experimental results fit nicely, and the model can be used to predict the amount of product formed. Also, it is possible to conclude that the kinetic parameters described the system well for the operative conditions of interest. In order to consider more diverse cases, V_{max} and K_m at different operative conditions (e.g. different amount of catalyst) need to be experimentally determined.

6. Conclusions

The present work involved the synthesis of nanoreactors with the intention of preserving their activity when employing them in flow with the possibility of reusing them, therefore proving a nanoreactor's capability of protecting the enzyme. Despite their protective property, making them suitable for larger scale processes involves assuring that nanoreactors also possess improved kinetic properties when compared to the free enzyme. According to literature, Candida Antarctica Lipase B (Cal B) seemed appropriate for industrial catalysis, encouraging to pursue this research by selecting this enzyme to develop novel catalytic nanosystems and employ them in a continuous flow system, thereby making progress in scaling up the applicability of nanoreactors.

The bibliographical review carried out on the main topics under study was supposed to make the reader aware of the research matter and also give a sense of how the experimental procedure should progress and an idea on what to expect from this dissertation.

The nanoreactors synthesized attained an adequate shape and distribution, since the aim was to obtain polymeric vesicles and the encapsulation had a positive effect on the enzyme's activity and kinetic properties particularly characterized by a high turnover number. In fact, this feature prompted the use of nanoreactors in flow.

The major conclusions that could be drawn from the flow experiments are that an encapsulated enzyme's activity can be preserved in flow and its reusability is possible. This study demonstrated that a nanoreactor is capable of protecting the enzyme encapsulated within it and aside from this it also showed that Cal B-catalyzed conversion could present an improved reaction performance when Cal B is in its encapsulated form. While studying the effect of Cal B loaded nanoreactors in flow, it was found that using a lesser load attained a reduced leaching, but it obviously decreased the productivity. On the other hand, an intermediate load is preferable compared to a higher load due to the occurrence of mass transfer limitations when a high amount of catalyst is present, however leaching being an aspect that needs to be improved. Nevertheless, the product outcome was improved by promoting a better contact between the enzyme and the substrate using a milli-flow device and decreasing the diffusional limitations. Using a milli-flow device to conduct a reaction and to employ the Cal B nanoreactors, while also recycling them to minimize the reaction waste and cut costs is perceived as a sustainable method.

The development of a numerical model in MATLAB©, using parameters obtained experimentally to reproduce the kinetic data collected, and predict a reaction's performance showed that the model results fitted the experimental tests that used a higher concentration of substrate to a greater degree. This also can ensure if productivity goals are met.

Finally, a nanoreactors' contribution in obtaining higher yields and decreasing reaction waste, as observed, highlighted its potential for green processing on a larger scale and could be one of the solutions for sustainable development envisioned by many industries.

7. Future Directions

Future work will be aimed at addressing some of the shortcomings of the current nanoreactors' performance and extending the ideas explored in this present study to industrial applications.

Although this work contributed for advancements in intersecting the field of industrial catalysis with nanoscience and also for process intensification, some challenges still endure. As mentioned above it will be important to improve the leaching and, therefore, also extending the reusability of the nanoreactors in flow, which could be beneficial for industries. The leaching is an aspect that could be solved by crosslinking the membrane of the Cal B stomatocytes thereby increasing their stability by making them more resistant to leaching, meaning that the catalyst would possibly be retained within the supramolecular assembly, leading to higher yields even after being used a considerable number of times.

The mathematical model developed using the kinetic parameters determined experimentally could be used to optimize the processes conducted using different conditions, therefore offering more operative conditions to work within a lab setting.

Prior to this research, it was found that the use of static mixers could be valuable when attempting to scale up a process. The presence of this type of device within a flow setup could definitely potentiate the continuous mixing of fluids consisting of a reliable possibility to achieve better product outcomes. In fact, it could promote a better contact between the nanoreactors and the substrate, especially if enclosed in the bigger flow setup used in this research, since the lack of contact between the enzyme and substrate is one of the reasons of a lower reaction performance. In this case, a helical static mixer would be recommended since the reaction mixture was not viscous.

Furthermore, the encapsulation of other enzymes relevant for industrial applications, following the entrapment method presented, could also be useful for process intensification which broadens the scope of this work for future chemical process applications.

8. References

[1] Che H and van Hest J C M 2016 Stimuli-responsive polymersomes and nanoreactors *J. Mater. Chem. B* **4** 4632–47

[2] Gaitzsch J, Huang X and Voit B 2016 Engineering Functional Polymer Capsules toward Smart Nanoreactors *Chem. Rev.* **116** 1053–93

[3] Vriezema D M, Garcia P M L, Sancho Oltra N, Hatzakis N S, Kuiper S M, Nolte R J M, Rowan A E and Van Hest J C M 2007 Positional assembly of enzymes in polymersome nanoreactors for cascade reactions *Angew. Chemie - Int. Ed.* **46** 7378–82

[4] Peters R J R W, Marguet M, Marais S, Fraaije M W, Van Hest J C M and Lecommandoux S 2014 Cascade reactions in multicompartmentalized polymersomes *Angew. Chemie - Int. Ed.* **53** 146–50

[5] van Oers M C M, Rutjes F P J T and Van Hest J C M 2014 Cascade reactions in nanoreactors *Curr. Opin. Biotechnol.* **28** 10–6

[6] Abdelmohsen L K E A, Nijemeisland M, Pawar G M, Janssen G J A, Nolte R J M, Van Hest J C M and Wilson D A 2016 Dynamic Loading and Unloading of Proteins in Polymeric Stomatocytes: Formation of an Enzyme-Loaded Supramolecular Nanomotor *ACS Nano* **10** 2652–60

[7] De Martino M T, Abdelmohsen L K E A, Rutjes F P J T and Van Hest J C M 2018 Nanoreactors for green catalysis *Beilstein J. Org. Chem.* **14** 716–33

[8] Nicolaou K C, Edmonds D J and Bulger P G 2006 Cascade reactions in total synthesis *Angew. Chemie - Int. Ed.* **45** 7134–86

[9] Tufvesson P, Fu W, Jensen J S and Woodley J M 2010 Process considerations for the scale-up and implementation of biocatalysis *Food Bioprod. Process.* **88** 3–11

[10] Wilson D A, Nolte R J M and Van Hest J C M 2012 Entrapment of metal nanoparticles in polymer stomatocytes *J. Am. Chem. Soc.* **134** 9894–7

[11] Rikken R S M, Engelkamp H, Nolte R J M, Maan J C, Van Hest J C M, Wilson D A and Christianen P C M 2016 Shaping polymersomes into predictable morphologies via out-of-equilibrium self-assembly *Nat. Commun.* **7** 1–7

[12] Men Y, Peng F, Tu Y, Van Hest J C M and Wilson D A 2016 Methods for production of uniform small-sized polymersome with rigid membrane *Polym. Chem.* **7** 3977–82

[13] Iyisan B 2016 Multifunctional and Stimuli-Responsive Polymersomes for Biomedical Applications

[14] Kuiper S M, Nallani M, Vriezema D M, Cornelissen, Van Hest J C M, Nolte R J M and Rowan A E 2008 Enzymes containing porous polymersomes as nano reaction vessels for cascade reactions *Org. Biomol. Chem.* **6** 4315–8

[15] Pramanik P and Ghosh S 2015 Thermoresponsive polymersome from a double hydrophilic block copolymer *J. Polym. Sci. Part A Polym. Chem.* **53** 2444–51

[16] Pijpers I A B, Abdelmohsen L K E A, Williams D S and Van Hest J C M 2017 Morphology under Control: Engineering Biodegradable Stomatocytes *ACS Macro Lett.* **6** 1217–22

[17] Kim K T, Zhu J, Meeuwissen S A, Cornelissen J J L M, Pochan D J, Nolte R J M and Van Hest J C M 2010 Polymersome stomatocytes: Controlled shape transformation in polymer vesicles *J. Am. Chem. Soc.* **132** 12522–4

[18] Palivan C G, Goers R, Najer A, Zhang X, Car A and Meier W 2016 Bioinspired polymer vesicles and membranes for biological and medical applications *Chem. Soc. Rev.* **45** 377–411

[19] Tanner P, Baumann P, Enea R, Onaca O, Palivan C and Meier W 2011 Polymeric vesicles: From drug carriers to nanoreactors and artificial organelles *Acc. Chem. Res.* **44** 1039–49

[20] van Oers M C M, Veldmate W S, van Hest J C M and Rutjes F P J T 2015 Aqueous asymmetric aldol reactions in polymersome membranes *Polym. Chem.* **6** 5358–61

[21] Handayani N, Miletic N, Loos K, Achmad S and Wahyuningrum D 2011 Properties of immobilized Candida antarctica lipase B on highly macroporous copolymer *Sains Malaysiana* **40** 965–72

[22] Watts P and Wiles C 2012 Micro reactors, flow reactors and continuous flow synthesis *J. Chem. Res.* **36** 181–93

[23] Wiles C and Watts P 2012 Continuous flow reactors: a perspective *Green Chem.* **14** 38–54
[24] Ostafin A and Chen Y-C Nanoreactors pp 1–18
[25] McQuade D T and Seeberger P H 2013 Applying Flow Chemistry: Methods, Materials, and Multistep Synthesis *J. Org. Chem.* **78** 6384–9
[26] Denčić I, De Vaan S, Noël T, Meuldijk J, De Croon M and Hessel V 2013 Lipase-based biocatalytic flow process in a packed-bed microreactor *Ind. Eng. Chem. Res.* **52** 10951–60
[27] Mason M https://www.environmentalscience.org/sustainability
[28] Vriezema D M, Aragonès M C, Elemans J A A W, Cornelissen J J L M, Rowan A E and Nolte R J M 2005 Self-assembled nanoreactors *Chem. Rev.* **105** 1445–89
[29] Katsuhiko Ariga 2007 Layer-by-layer assembly as a versatile bottom-up nanofabrication technique for exploratory research and realistic application *R. Soc. Chem.* 2319–2340
[30] Park C, Yoon J and Thomas E L 2003 Enabling nanotechnology with self assembled block copolymer patterns **44** 6725–60
[31] Förster, Stephan and Konrad M 2003 From self-organizing polymers to nano- and biomaterials *J. Mater. Chem.* **13** 2671–88
[32] Palivan 2013 Polymer Nanoreactors pp 1–31
[33] Discher D E and Ahmed F 2006 Polymersomes **8** 323–41
[34] Du J 2014 Polymer Vesicles *Adv. Hierarchical Nanostructured Mater.* **9783527333** 177–92
[35] Chang H-Y, Sheng Y-J and Tsao H-K 2014 Structural and mechanical characteristics of polymersomes *Soft Matter* **10** 6373
[36] Schoonen L and Van Hest J C M 2016 Compartmentalization Approaches in Soft Matter Science: From Nanoreactor Development to Organelle Mimics *Adv. Mater.* **28** 1109–28
[37] Goodsell D S 2004 *Bionanotechnology: Lessons from Nature*
[38] Wood 2017 Metallic bionanocatalysts: potential applications as green catalysts and energy materials *Microb. Biotechnlogy* **10** 1171–80
[39] Hagen J 2015 *Industrial Catalysis: A Practical Approach* (John Wiley & Sons)
[40] BRAZIL R 2018 Combining homogeneous and heterogeneous catalysis
[41] Dergunov S A, Khabiyev A T, Shmakov S N, Kim M D, Ehterami N, Weiss M C, Birman V B and Pinkhassik E 2016 Encapsulation of Homogeneous Catalysts in Porous Polymer Nanocapsules Produces Fast-Acting Selective Nanoreactors *ACS Nano* **10** 11397–406
[42] Klermund L, Poschenrieder S T and Castiglione K 2017 Biocatalysis in Polymersomes: Improving Multienzyme Cascades with Incompatible Reaction Steps by Compartmentalization *ACS Catal.* **7** 3900–4
[43] Grayson I 2016 Chemocatalysis or biocatalysis.pdf *Catalysis* **34**
[44] Anon 1986 Chapter 1: Introduction 2–32
[45] Adlercreutz P 2013 Immobilisation and application of lipases in organic media *Chem. Soc. Rev.* **42** 6406–36
[46] Anon https://en.wikipedia.org/wiki/Lipase#cite_note-28
[47] Bhangale A S, Beers K L and Gross R A 2012 Enzyme-Catalyzed Polymerization of End-Functionalized Polymers in a Microreactor *Macromolecules* **45** 7000–8
[48] Kundu S, Bhangale A S, Wallace W E, Flynn K M, Guttman C M, Gross R A and Beers K L 2011 Continuous Flow Enzyme-Catalyzed Polymerization in a Microreactor *J. Am. Chem. Soc.* **133** 6006–11
[49] Choi J M, Han S S and Kim H S 2015 Industrial applications of enzyme biocatalysis: Current status and future aspects *Biotechnol. Adv.* **33** 1443–54
[50] Feynman R P 1959 “Plenty of Room at the Bottom.” *Am. Phys. Soc.*
[51] Mukhtar M and Pillai U 2015 Nanomanufacturing: Application of nanotechnology in manufacturing industries *Nanotechnol. Law Bus.* **12** 5–18
[52] Choi B, Rempala G A and Kim J K 2017 Beyond the Michaelis-Menten equation: Accurate and efficient estimation of enzyme kinetic parameters *Sci. Rep.* **7** 1–11

[53] Carrillo N, Ceccarelli E A and Roveri O A 2010 Usefulness of kinetic enzyme parameters in biotechnological practice *Biotechnol. Genet. Eng. Rev.* **27** 367–82
[54] Kaul P and Asano Y 2012 Strategies for discovery and improvement of enzyme function: State of the art and opportunities *Microb. Biotechnol.* **5** 18–33
[55] Schaller C P (College of S B / S J U https://employees.csbsju.edu/cschaller/Reactivity/kinetics/arkenzymemath.htm
[56] Marques M P C and Fernandes P 2011 Microfluidic devices: Useful tools for bioprocess intensification *Molecules* **16** 8368–401
[57] Yoshida 2013 *Micro Process Engineering: A Comprehensive Handbook*
[58] Laurenti E and dos Santos Vianna Jr. A 2016 Enzymatic microreactors in biocatalysis: history, features, and future perspectives *Biocatalysis* **1** 148–65
[59] Sweetland B Elements of Chemical Reaction Engineering
[60] Gobert S R L, Kuhn S, Braeken L and Thomassen L C J 2017 Characterization of Milli- and Microflow Reactors: Mixing Efficiency and Residence Time Distribution *Org. Process Res. Dev.* **21** 531–42
[61] Kim K T, Cornelissen J J L M, Nolte R J M and Van Hest J C M 2009 A polymersome nanoreactor with controllable permeability induced by stimuli-responsive block copolymers *Adv. Mater.* **21** 2787–91
[62] Meurant G 2012 *Introduction to Dynamic Light Scattering by Macromolecules*
[63] https://www.wyatt.com/library/theory/dynamic-light-scattering-theory.html
[64] Instruments M Dynamic Light Scattering: An Introduction in 30 Minutes Introduction 1–8
[65] https://www.explainthatstuff.com/electronmicroscopes.html
[66] https://bitesizebio.com/29197/introduction-electron-microscopy-biologists/
[67] https://www.wyatt.com/library/theory/flow-field-flow-fractionation-theory.html
[68] Anon https://chem.libretexts.org/Textbook_Maps/Physical_and_Theoretical_Chemistry_Textbook_Maps/Supplemental_Modules_(Physical_and_Theoretical_Chemistry)/Kinetics/Reaction_Rates/Experimental_Determination_of_Kinetcs/Spectrophotometry
[69] Anon https://www.youtube.com/watch?v=hdb3s4YHkms&t=0s&index=7&list=PLej32UqTN1LzOGA18TuCJ7Jnv3c4lDI-l
[70] Anon http://www.howbiotech.com/the-principle-and-procedure-of-polyacrylamide-gel-electrophoresis-sds-page/
[71] Anon https://ww2.chemistry.gatech.edu/~lw26/course_Information/4581/techniques/gel_elect/page_protein.html
[72] Anon http://elte.prompt.hu/sites/default/files/tananyagok/IntroductionToPracticalBiochemistry/ch07s03.html
[73] Anon https://www.thermofisher.com/pt/en/home/life-science/protein-biology/protein-biology-learning-center/protein-biology-resource-library/pierce-protein-methods/protein-gel-stains.html
[74] Anon http://www.bio-rad.com/en-nl/applications-technologies/sds-page-analysis?ID=LW7FGX4VY
[75] Anon http://hiq.linde-gas.com/en/analytical_methods/liquid_chromatography/high_performance_liquid_chromatography.html
[76] Anon http://www.waters.com/waters/pt_PT/How-Does-High-Performance-Liquid-Chromatography-Work%3F/nav.htm?cid=10049055&locale=pt_PT
[77] A. Kayode Coker P D and Coker A. Kayode 2001 Modeling of Chemical Kinetics and Reactor Design *Model. Chem. Kinet. React. Des.* 260–423
[78] Rotticci D, Norin T and Hult K 2000 Mass transport limitations reduce the effective

stereospecificity in enzyme-catalyzed Kinetic Resolution *Org. Lett.* **2** 1373–6

[79] Online V A, Forsyth C and Patwardhan S V 2013 bioinspired silica † 1164–74

[80] De Hoog H P M, Arends I W C E, Rowan A E, Cornelissen J J L M and Nolte R J M 2010 A hydrogel-based enzyme-loaded polymersome reactor *Nanoscale* **2** 709–16

9. Appendices

Appendix A: Kinetic Model

The kinetic model using experimental values for this study was developed in MATLAB© and its development is described below.

```
clear
clc
global CS0 Km Vmax Cp0  Km2 Vmax2  Cp01

Cp0=0.07262;% mM
Cp01=0.292577;
CS0=1.2; %mM
Km=3.543;%mM
Vmax=0.0078;%mM/min
Km2=3.863;%mM
Vmax2= 0.03464;%mM/min



t=[0    1.123733333 2.24715 3.3712  4.495283333 5.618866667 6.7426  7.866183333
8.990066667 10.11388333 11.23786667 12.36151667 13.4849 14.60868333 15.73281667];
C0= [CS0 Cp0 CS0 Cp01];
[tx Cx]= ode45(@rates1,t,C0);
figure
plot(t,Cx)
title('Concentration profiles')
xlabel('Time (min)')
ylabel('Concentration (mM)')
hold on


grid on
legend('pNPA','pNP','pNPA_ (stoma)','pNP_
(stoma)','location','northeast')

----------------------------------------------------------

function dy=rates1(t,y)
global Km CS0 Vmax Cp0  Vmax2 Km2  dv
dy(1)=-((Vmax*y(1))/(y(1)+Km));
 dy(2)=((Vmax*(y(1)))/((y(1))+Km));
 dy(3)=-((Vmax2*y(3))/(y(3)+Km2));
 dy(4)=((Vmax2*(y(3)))/((y(3))+Km2));
 dy=dy';
```

Appendix B: Polymer PEG_{44}-PS_{140}

The amphiphilic block copolymer PEG_{44}-PS_{140} was produced by Atom Transfer Radical Polimerization (ATRP) and was used as building block for the polymersomes' self-assembly. Its synthesis is described below, based on previous works.

Copper bromide (CuBr) (45 mg, 0,32 mmol) was added to a dry Schlenk tube equipped with a stirring bar under argon atmosphere. The Schlenk tube was then sealed with a septum, evacuated for 15 min after which argon was filled back into a flask. PMDETA (66 µL, 0,32 mmol) was dissolved in 0,5 mL of anisole and added into the CuBr. The mixture was left stirring for 15 min with argon bubbling through the solution for oxygen removal. Subsequently, PEG macro initiator (215 mg, 0,10 mmol) was dissolved in 1 mL of anisole and added into the Schlenk tube. The Schlenk tube was inserted in an ice bath, and the solution was degassed for 15 min. Afterwards, distilled styrene (5 mL, 43,6 mmol) was inserted into the Schlenk tube. The mixture was degassed by three freeze thaw cycles after which the Schlenk tube was inserted into the preheated 70 ºC oil bath overnight. Dichloromethane (CH_2Cl_2) (75 mL) was then added into the polymer solution and the organic layer was extracted with aqueous 65 mM EDTA solution (3 x 150 mL). The aqueous phase was washed with CH_2Cl_2 and the organic layers were combined and dried with $MgSO_4$. The solution was then concentrated, and the polymer was precipitated in cold MeOH, filtered and dried overnight.

Appendix C: DLS measurements

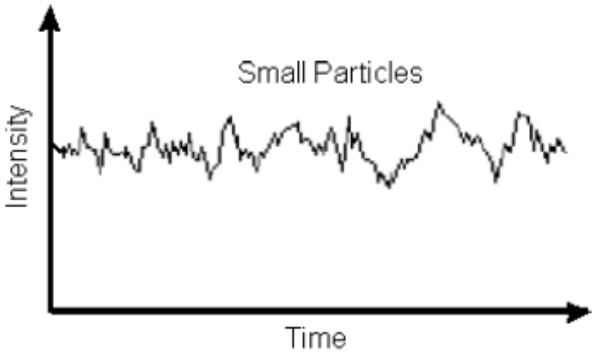

Figure 9.1- Typical intensity fluctuations for small particles.

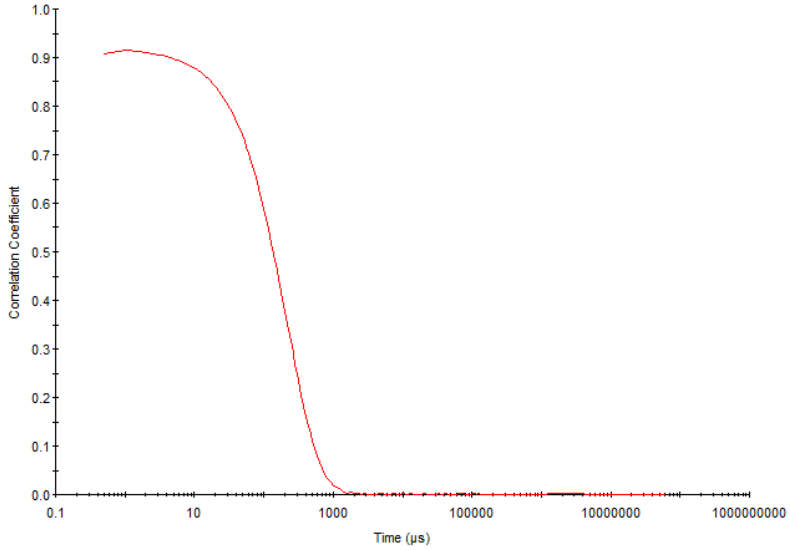

Figure 9.2- Correlogram obtained from the polymersomes sample.

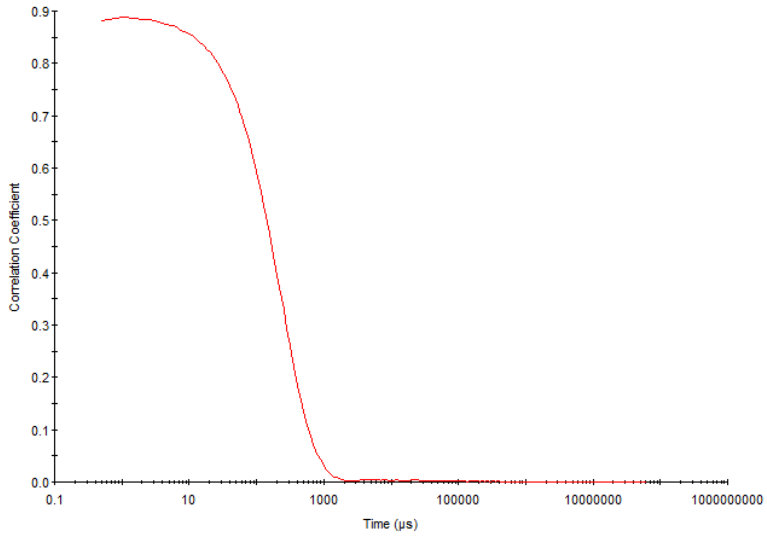

Figure 9.3- Correlogram obtained from the biocatalytic stomatocytes sample.

Appendix D: Enzyme Quantification

D1 Spectrophotometric assay

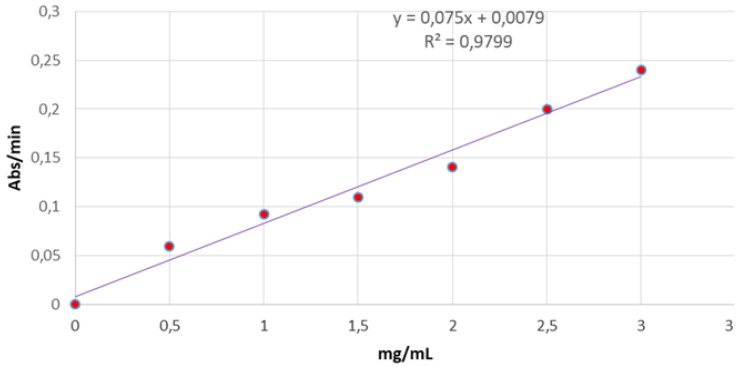

Figure 9.4- Calibration curve for Cal B from the enzymatic assay.

D2 Bradford assay

Table 9.1- Data obtained for Bradford assay calibration curve.

[BSA] (mg/mL)	Abs_{595nm}
2	1,229
1,5	1,021
0,75	0,604
0,5	0,434
0,25	0,264
0,125	0,144
0,025	0,066
0	0

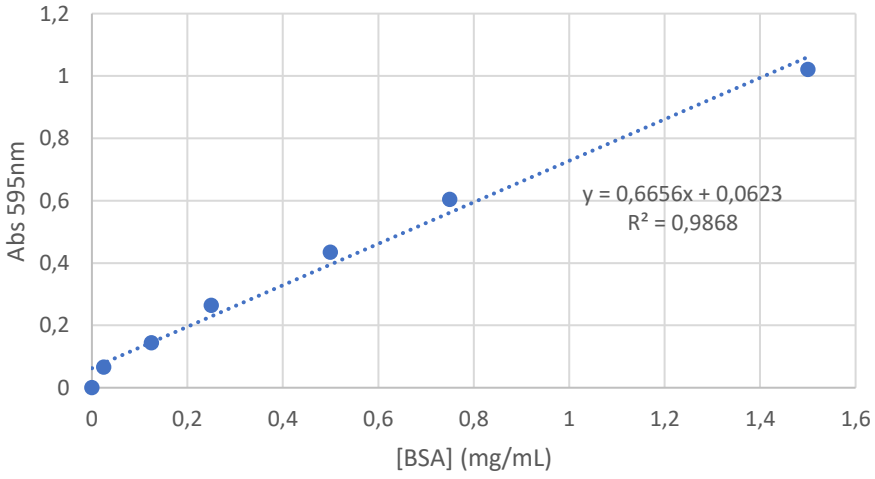

Figure 9.5- Bradford assay calibraton curve.

Table 9.2- Absorbance values measured at 595 nm and encapsulation efficiencies of catalytic stomatocytes samples.

Sample	Abs_{595nm}	Encapsulation efficiency(%)
1	0,2586 0,2612 0,2588	32,9±0,2
2	0,0995 0,09354	5,7±0,7
3	0,1382 0,1262 0,1369	12±1
4	0,1902 0,1989 0,1968	22,2±0,8
5	0,1150 0,1160 0,1167	8,9±0,1
6	0,1360 0,1539 0,1538	14±2

Appendix E: Enzymatic Activity

The enzymatic activity for Cal B in its free form was measured by conducting a spectrophotometric assay described in section 4.3.1.1.

Table 9.3- Specific activity values for free Cal B based on two spectrophotometric assays.

Assay	ΔAbs_{CalB}	ΔAbs_{CalB}-ΔAbs_{BG}	ΔAbs	Cal B (mg)	U_{total}	Activity (U/mg)
Test 1	0,0022	0,0022	0,13	0,09	1,76	19,5
Test 2	0,0027	0,0026	0,16	0,09	2,12	23,5

A volume of 36 µL was used as catalyst for the test reaction from a 2,5 mg/mL solution of Cal B to determine the free enzyme activity, meaning that there is 0,09 mg of Cal B present.

Appendix F: Kinetic study

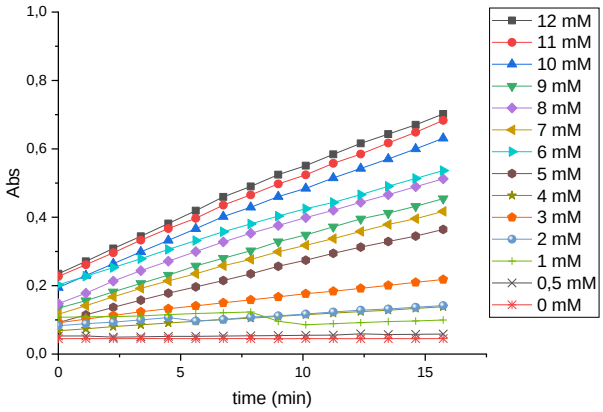

Figure 9.6- Activity of free Cal B catalyzed conversion of p-nitrophenyl acetate to p-nitrophenol.

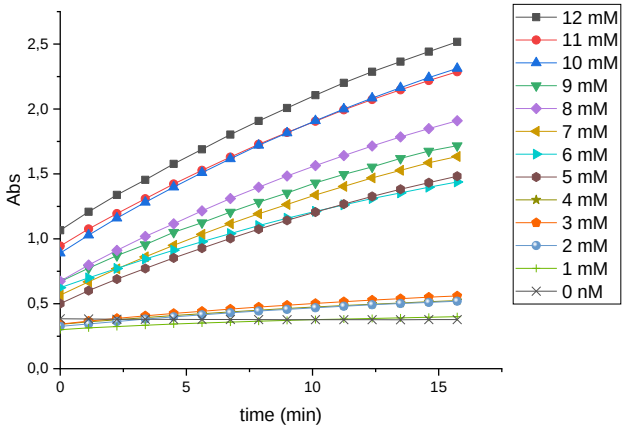

Figure 9.7- Activity of encapsulated Cal B catalyzed conversion of p-nitrophenyl acetate to p-nitrophenol.

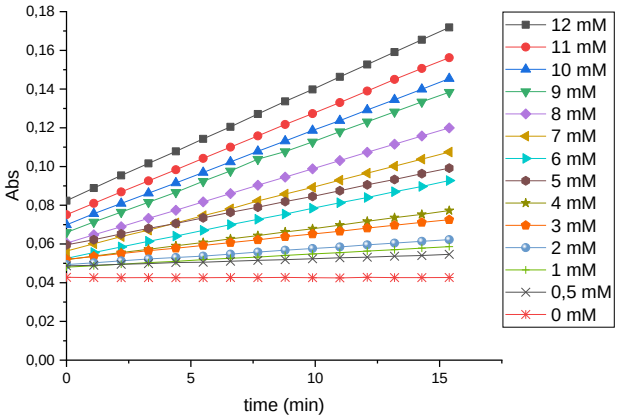

Figure 9.8- Activity of non-catalyzed conversion of p-nitrophenyl acetate to p-nitrophenol.

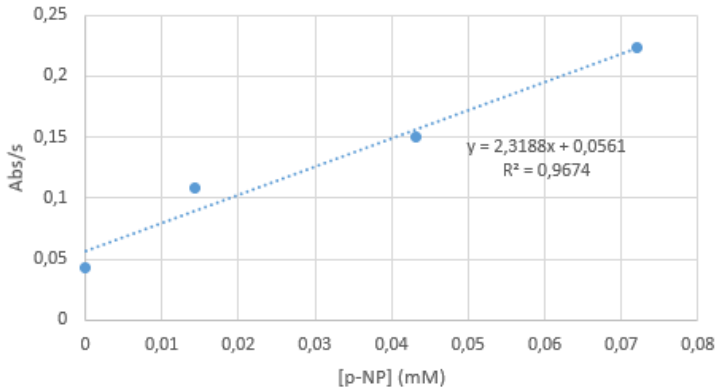

Figure 9.9- Calibration curve for p-nitrophenol based on its absorbance at different concentrations.

Table 9.4- Enzymatic data obtained from spectrophotometric assay (higher substrate concentrations).

[p-NPA] (mM)	12	11	10	9	8	7	6
free enzyme	1,03E-02	1,00E-02	9,67E-03	6,80E-03	8,14E-03	6,67E-03	7,94E-03
stomatocytes	3,71E-02	3,44E-02	3,66E-02	2,68E-02	3,20E-02	2,78E-02	2,13E-02

Table 9.5- Enzymatic data obtained from spectrophotometric assay (lower substrate concentrations).

[p-NPA] (mM)	5	4	3	2	1	0,5	0
free enzyme	6,28E-03	1,17E-03	2,82E-03	1,15E-03	-9,13E-04	5,25E-05	0
stomatocytes	2,56E-02	4,40E-03	5,43E-03	5,06E-03	2,47E-03	-	0

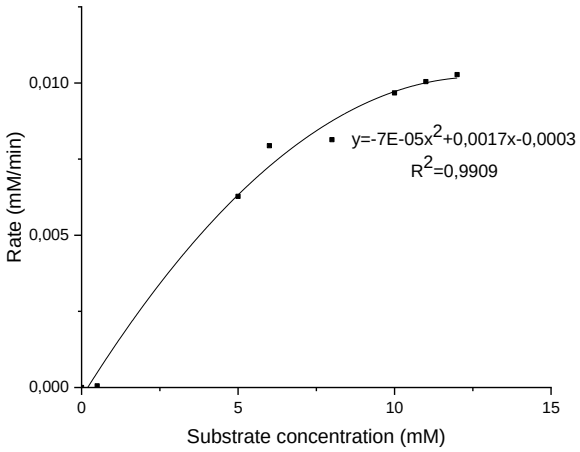

Figure 9.10- Saturation curve for free Cal B.

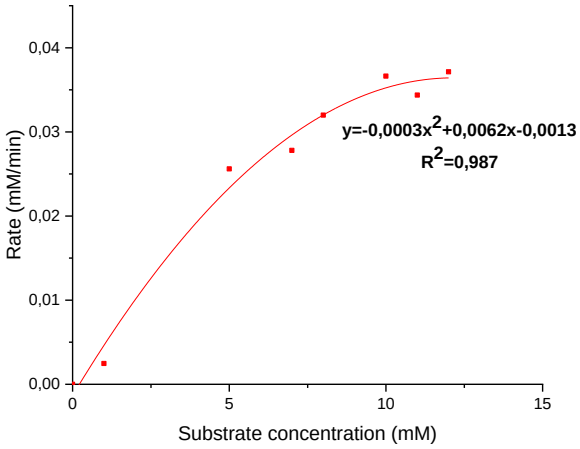

Figure 9.11- Saturation curve for encapsulated Cal B.

Appendix G: Product Quantification

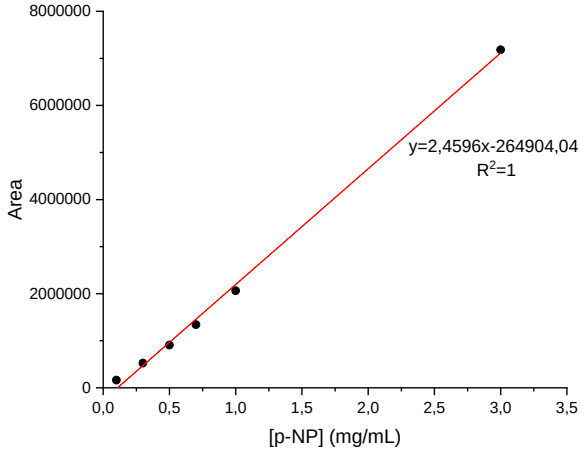

Figure 9.12- Product calibration curve using HPLC.

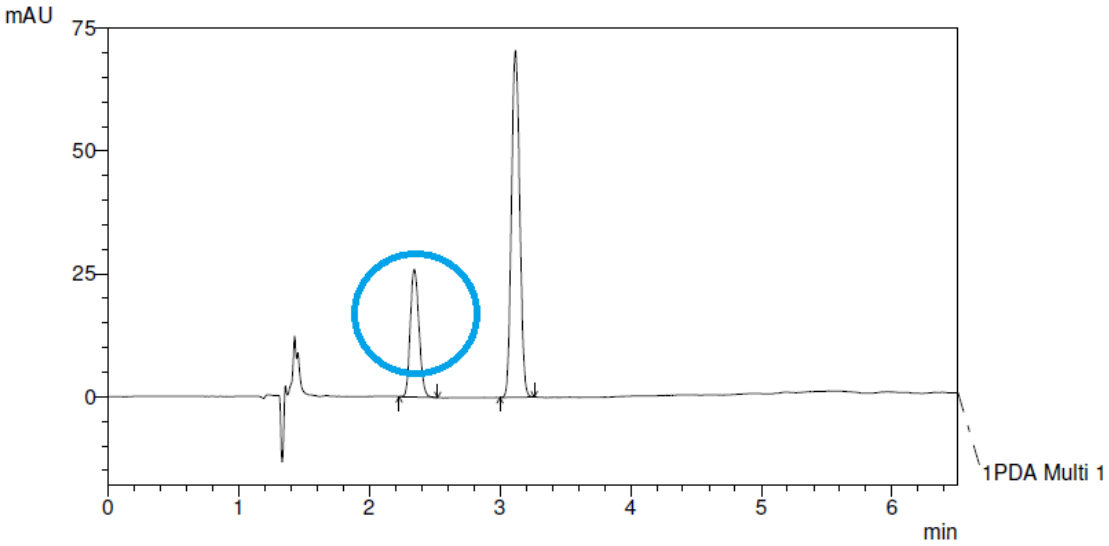

Figure 9.13- Example of a chromatogram of a sample collected at the outlet of the milli-flow reactor. The circled peak corresponds to the peak of the desired product (p-NP).

Table 9.6- Yields of product obtained when studying the effects of encapsulation in both flow setups.

	Cal B form	Peak area	m p-NP (mg)	n p-NP (mmol)	Y p-NP (%)
Smaller reactor	free	2,64E+04	0,15	1,05E-03	53,4
	encapsulated	9,09E+05	0,19	1,39E-03	69,8
Bigger reactor	free	2,69E+04	0,26	1,87E-03	8,3
	encapsulated	2,55E+05	0,29	2,10E-03	9,3

Table 9.7- Relative activity calculated for leaching experiments using different Cal B loaded nanoreactors.

Cycle of reuse	1	2	3	4	5
33% load	64,3	37,4	25,3	23,3	20,4
6% load	94,8	35,2	27,8	28,0	22,9
14% load	97,8	56,7	58,7	50,7	-